2007

Determining the AGN Fraction of Galaxy Groups

Rachel Paterno-Mahler
Pomona College

Determining the AGN Fraction of Galaxy Groups

Rachel Paterno-Mahler

Advisor: Philip Choi

A thesis submitted in partial fulfillment of the

requirements for the degree of

Bachelor of Arts in Physics

Pomona College

May 2, 2007

Contents

Abstract

We combined publicly available archival European Photon Imaging Camera (EPIC) data from XMM-Newton X-ray observatory with ground-based optical and near-infrared datasets to measure the Active Galactic Nuclei (AGN) fraction of nine low-redshift ($z < 0.05$) galaxy groups. Using SAS to reduce the X-ray images, we catalogued 30 X-ray group members, three of which we identified as AGN based primarily on their X-ray luminosities $L_X \geq 10^{41}$ erg/s. These luminosities are consistent with the X-ray luminosities of AGN. For galaxies with $M_R < -20$, we derive a group AGN fraction $f_A = 11.1^{+13.6}_{-7.0}\%$ as compared to $f_A = 5 \pm 1.5\%$ for galaxy clusters (Martini et al., 2006).

CHAPTER 1

Introduction

Using the Chandra X-ray Observatory, Martini et al. (2006) found that the AGN fraction of galaxy clusters was five times higher than previous optical studies suggested. Using visual observations only, Dressler et al. (1985) estimated the AGN fraction of field galaxies to be 5%, while that of clusters was thought to be 1%. A field galaxy is a galaxy that is not associated with any other galaxy. After their survey, Martini et al. (2006) calculated the AGN (Active Galactic Nuclei) fraction of clusters to be 5% using X-ray observations in addition to visual ones. This has interesting implications. If these ratios were kept the same, then the AGN fraction of the field would then be increased to 25% (Martini et al., 2006). This presumes that the AGN fraction of clusters really is less than the field. There are two reasons that the optical data might vary from the X-ray data. First, the stellar light of the host galaxy may dilute the optical emission lines of the AGN. Second, there may be a high column density of dust in the region of activity. Both of these will likely obscure optical observations but are generally not problems when observing in the X-ray part of the spectrum.

To understand the role that the environment plays in AGN fueling, we must study a variety of environments, ranging from the field to groups to clusters. Will the AGN fraction of groups also be higher than that of the field? We would also like to see how the AGN fraction of groups compares to that of clusters. In the following sections, I will describe the mechanics of X-ray astronomy, the group

environment, and the characteristics of active galactic nuclei. I will also briefly describe the possible mechanisms for AGN fueling.

1. X-ray Astronomy

X-ray astronomy has become possible due to the advent of satellite technology in the 1970s. Save for ultraviolet (UV) radiation, X-ray radiation was the last region of the electromagnetic spectrum to be explored. X-rays range in energy from $10^2 - 10^4$ eV and have wavelengths between 0.1 and 10 nm. In astronomy, they are used to observe high-energy objects. Low energy X-rays are called soft X-rays, while higher energy ones are called hard X-rays (Karttunen et al., 2003). Hard X-rays are those that have energies higher than 2 keV. Although X-rays are highly energetic, the thickness of the atmosphere means that all incoming photons are easily scattered and absorbed. Because of this, ground based X-ray observatories are not possible (Tucker and Giacconi, 1985).

The first X-ray telescope, UHURU [1], was launched in 1970. Because of the high energies of the photons, optical observational methods are not sufficient to collect the light. Traditional glass mirrors are not useable, since X-rays will pass straight through the glass if the beam is perpendicular to the mirror's surface (Carroll and Ostlie, 2007). Incoming X-ray photons can, however, be focused if they hit the reflecting surface at grazing angles of less than one degree. Because of the very small grazing angle, the reflecting surface must be nearly parallel to the incoming beam, as shown in Figure 1.1. These telescopes are shaped like cylindrical tubes, rather than the standard dish shape of radio or optical telescopes, and many tubes tend to be nestled within one another (Tucker and Giacconi, 1985). The photons are then detected by Geiger-Müller counters, proportional counters, or

[1] Also known as the Small Astronomy Satellite-1, SAS-1

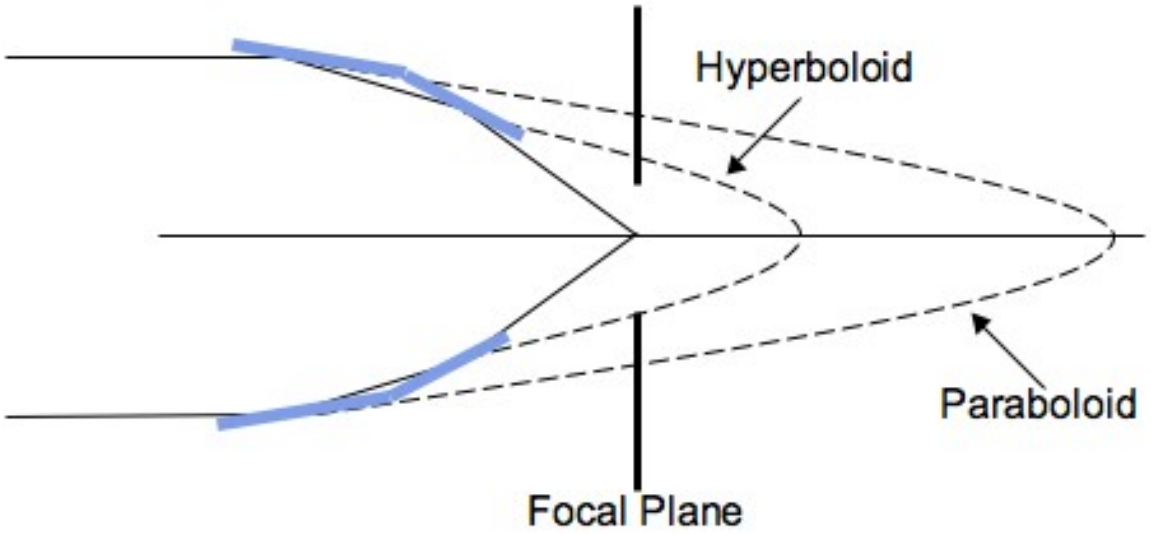

Figure 1.1: The incoming X-rays graze the surface of the paraboloid mirror and are reflected onto the hyperboloid mirror and are focused to a point.

scintillation detectors. The first two detectors are boxes filled with gas, with the walls of the detector forming a cathode and an anode wire running through the middle. When the X-rays hit the gas particles, the particles are ionized, and the potential difference between the walls of the box and the wire causes a current (Karttunen et al., 2003). The Geiger-Müller and proportional counters are very similar to each other; however, they have different operating voltages. Additionally, a proportional counter measures the amount of energy deposited, while a Geiger-Müller counter only measures whether or not a photon has hit the detector. A scintillation detector consists of a scintillating material and a photomultiplier. When the incoming electrons strike the scintillating material, its atoms or molecules are excited, which causes light to be emitted. This light is transmitted to the photomultiplier, where it is converted to a weak current and then amplified so that it can be analyzed (Leo, 1988). The detectors integrate for long periods of time (generally between 10^3 and 10^5 s), since the frequency of

X-ray counts tends to be low compared with photon counts from other parts of the spectrum.

Currently there are two X-ray observatories in orbit—the Chandra X-ray Observatory, which was launched in 1999 and is operated for NASA by the Smithsonian Astrophysical Observatory, and the X-ray Multi-Mirror Newton Observatory (XMM-Newton), which the European Space Agency launched in December of 1999. Here I will focus on XMM-Newton, since it is the observatory used in this study. XMM-Newton is most sensitive in the energy range 0.25 – 12 keV. XMM-Newton has three European Photon Imaging Cameras (EPIC)—two of which are MOS detectors and one of which is a PN detector. All three cameras operate in photon counting mode, which produces an event list. This allows for simultaneous imaging and spectroscopy (Dahlem, 1999). The two MOS detectors are rotated 90° with respect to each other. All three detectors have a 30-arcminute field of view. In the PN CCD, the photons hit the detector from the rear, making it different from the MOS CCDs (Strüder et al., 2001). This affects the quantum efficiency of the detectors—the PN camera can detect photons with high efficiency up to 15 keV (Dahlem, 1999). In addition to the three detectors, XMM-Newton also has two reflection grating spectrometers and an optical monitor.

2. Galaxy Groups

Most galaxies in the universe are found in associations with each other, whether in a cluster or a group. These systems are gravitationally bound, each individual member orbits about the center of mass, and they interact more with each other than the rest of the universe (Barnes, 2001). Most galaxies are found in associations called “groups” (Karttunen et al., 2003). While groups are smaller than clusters, the distinction between the two is not definite. In general, however,

groups tend to have fewer than 50 galaxies, with a diameter of approximately two Mpc and an average mass of approximately $3 \times 10^{13} M_{\odot}$, where $M_{\odot}$ is one solar mass. The velocity dispersions of groups tend to be comparable to the velocity dispersions of individual galaxies and much lower than those of clusters. This leads to a higher frequency of galaxy mergers in groups than in clusters (Mulchaey, 2000). In addition to each galaxy interacting with the other galaxies in the group, the galaxies interact with the gravitational potential of the group as a whole, which has a strong effect on galaxy properties. Studying these groups may provide information about the evolution of isolated galaxies and the relationship these galaxies have to those evolving in the cluster environment.

Although we know quite a bit about our own Local Group, the make-up of galaxy groups is generally not well studied, as most efforts to explore the morphologies of galaxies and their environment tend to focus on clusters. This is unfortunate, given that most galaxies undergo much of their evolution in the group environment (Barnes, 1985). This dearth of information is partly because it is difficult to construct theories for the evolution of these groups, since there are very few approximations one can make to simplify calculations (Barnes, 1985). The study of galaxy groups has also been slowed by small sample size, as most groups contain fewer than five galaxies (Zabludoff and Mulchaey, 1998).

While groups can be challenging to study, they can nominally be considered scaled-down versions of rich clusters (Mulchaey, 2000). Studies have found that groups have a higher fraction of early-type (bulge dominated) galaxies than the field (50% for groups as compared with 17% in the field). Field galaxies are galaxies that exist outside of the group or cluster environment. These observations are consistent with predictions that more massive galaxies form in denser

regions (Tran et al., 2001). X-ray detected groups tend to have higher velocity dispersions and early-type galaxy fractions than non X-ray detected groups (Zabludoff and Mulchaey, 1998). Because of this, groups are probable sites for interactions and mergers. Interestingly, however, in the disk-dominated groups, the fraction of asymmetric galaxies, as well as star-forming galaxies, is lower than that of the field, as mergers that increase star formation and asymmetry are less likely to occur. There are two reasons for this. First, since early type galaxies dominate in groups, the chance of two gas-rich galaxies merging in the current epoch is reduced. Second, most of the group mass is contained in a common halo rather than with the galaxies, which reduces the cross-section of the galaxies and thus the merger rate (Tran et al., 2001). One way to study the evolution of galaxies in the group setting is to observe groups at different redshifts. The light we receive from higher redshift galaxies left those galaxies when they were younger in the earlier stages of evolution. Lower redshift groups are generally older and they have had more time to evolve.

Many galaxy groups have spatially extended X-ray emission, which comes from a hot, low-density gas known the intragroup medium. The peak of the X-ray emission is centered on the group's luminous central galaxy (Mulchaey, 2000). The central galaxy is indistinguishable from the center of the group's gravitational potential, which indicates that these large central galaxies may result from galaxy-galaxy mergers. This X-ray gas and its relationship to the central elliptical galaxy imply that the systems are real and not just superpositions of unbound galaxies, which was previously thought of galaxy groups. Also, the giant central elliptical galaxy that is present in the majority of groups is uncommon for field galaxies, giving further evidence that these groups are real (Zabludoff and Mulchaey, 1998).

Morphologically, groups that are spiral-rich tend to not contain a diffuse X-ray component, although many are X-ray sources (Mulchaey, 2000).

3. Active Galactic Nuclei

Edward A. Fath observed the first AGN in 1908 when he was looking at the spectra of spiral galaxies. One of his targets displayed six bright emission lines, rather than the standard absorption line spectrum produced by the galaxy's stars. This galaxy was later classified as a Seyfert galaxy, which is just one of the types of AGN (Carroll and Ostlie, 2007). The term AGN now refers to galaxy nuclei that exhibit anomalous energy output when compared to the expected energy output of a "normal" mixture of stars and gas (Shlosman et al., 1990). In addition to their distinct spectrum, the host galaxy is sometimes overwhelmed by the violent activity in the nucleus, which can outshine the entire galaxy. This causes the AGN to appear as a point source in images. Occasionally, jets are observed coming out of the nucleus. It is unlikely that such a high level of energy output could be sustained for long periods of time, which is why it appears that AGN are one stage of evolution for normal galaxies (Karttunen et al., 2003). The energy output of the AGN can also vary on timescales that range from hours to years. Their large energy output makes AGN excellent candidates for X-ray observations. Because both star formation and accretion onto the central super-massive black hole requires a reservoir of cold gas, the presence of nuclear activity in associations of galaxies is an indication of the efficiency with which the galaxies were stripped of the cold interstellar medium surrounding them and of how much growth the galaxy can continue to undergo in such an environment (Martini et al., 2002).

Although AGN occasionally appear as point sources, their spectral energy distribution (SED) is decidedly different from that of stars. Stars emit radiation as

blackbodies, while AGN have a power law emission to first order. A power law takes the form $f(x) = x^k$, where k is some exponent. They actually have a composite SED, with both power law emission and a thermal (blackbody) component, called the "big blue bump." This is an emission peak in the blue part of the visible spectrum, and it is associated with the accretion disk (Carroll and Ostlie, 2007). The power-law spectrum is characteristic of synchrotron radiation. Because of the wide SED, AGN are observable in many wavelengths of light.

While it is unknown what fuels the AGN, one model suggests that the activity is caused by the material of an accretion disk falling into a super-massive black hole at the center of the galaxy. An accretion disk is necessary because a black hole does not have a surface for material to fall on to. As matter spirals in through an accretion disk, however, a large fraction of the rest energy can be released as viscosity converts kinetic energy into heat and radiation (Carroll and Ostlie, 2007). This is done with some efficiency η, so the energy available is $E = \eta Mc^2$. The luminosity ($L = dE/dt$) is then

$$L = \eta \dot{M} c^2, \tag{1.1}$$

where $\dot{M}$ is the mass accretion rate. Whether or not accretion is a viable energy source depends on how large η is (Peterson, 1997).

Despite this model, it is unclear exactly how the mass gets converted into energy. It is possible that infalling matter can be transferred either through a hot ($T >> 10^4 K$) accretion flow, or through an alternative type of flow where the disk is composed of randomly moving clouds of gas embedded in a low-density medium. This latter alternative is the disk of clouds. The hot accretion flow requires pressures two to three orders of magnitude above that of the Interstellar Medium (ISM)

to be able to fuel an AGN without exceeding the virial temperature [2]. This is an efficient way of powering AGN if angular momentum transport is efficient; however idealized models of quasi-continuous accretion flows can run into serious problems. An alternative type of flow consists of a disk composed of randomly moving clouds of gas. Angular momentum transport entails viscous dissipation due to cloud collisions. The gas pressure of these clouds would have to be strongly dominated by magnetic energy (Shlosman et al., 1990). AGN can also be fueled when galaxies merge, which shocks the gas and can cause a larger amount of material to fall onto the black hole (Martini et al., 2006). In addition to these extrinsic interactions (which also include tidal encounters and orbital torques due to satellites), there are intrinsic interactions as well. These include instabilities brought on by the evolution of the disk. Such large-scale, non-local triggers avoid the constraints that local mechanisms of accretion place on the effective viscosity (Shlosman et al., 1990).

The accretion powered model of AGN fueling is consistent with the idea that there are many different types of AGN, including quasars and blazars. The different types of AGN depend on the galaxy's orientation with respect to the earth. A blazar has its spin axis pointing directly towards the Earth, whereas an AGN has its spin axis perpendicular to the Earth, although recently the term AGN has come to refer to nearly any galaxy with an active nucleus. The spin axis of quasars is oriented at angles between these two extremes. Here we do not differentiate between the different kinds of AGN.

Another, albeit less likely, fueling scenario is the nuclear starburst scenario. In this situation there is a dense star cluster (approximately 10^9 stars) sitting at

[2]The virial temperature can be calculated by substituting $K = 3kT/2$ into the virial theorem: $2K + U = 0$ (Peterson, 1997).

the center of the galaxy ($r \leq 10$ pc). The challenge is to explain how the stars get to such a close distance. Additionally, these star clusters cannot be the result of evolution by two-body relaxation, as collisions between stars would destroy the cluster. It is possible that a dynamic process such as a galaxy merger could trigger star formation in the nucleus, leading to a very dense cluster. Such clusters might evolve and merge to form a moderately large black hole. Problems arise, though, since one must assume the existence of a dense and massive cluster *a priori*. Angular momentum transport is also problematic in this model (Shlosman et al., 1990). This model is also not able to explain either rapid X-ray variability or radio-loud objects. Because AGN remain unresolved, the star cluster would have to be quite compact to remain unresolvable at the limits of the Hubble Space Telescope (Peterson, 1997)

In this paper we use X-ray observations to explore the AGN fraction of galaxy groups to see if it differs from that of galaxy clusters. As mentioned above, one possible explanation for AGN fueling is galaxy-galaxy mergers. Since groups of galaxies have lower velocity dispersions than clusters, one would expect a higher number of these galaxy mergers, which in turn would lead to a higher AGN fraction when compared with the AGN fraction of clusters. The observations and data reduction process are described in §2, while analysis of the images is described in §3. The results and their implications will be discussed in §4. Throughout, a flat ΛCDM cosmology with $\Omega_M = 0.3$, $\Omega_\Lambda = 0.7$ and $H_0 = 72\ km\ s^{-1}\ Mpc^{-1}$ is assumed.

CHAPTER 2

Data Reduction

1. The Galaxy Group Sample and XMM-Newton Dataset

We looked at nine different low redshift ($z < 0.05$) galaxy groups in the X-ray band—NGC 533, NGC 741, NGC 2563, HCG 42, HCG 62, HCG 90, NGC 5129, NGC 5846, and NGC 4325. Originally the sample also included NGC 7582, but it was missing its attitude data file so we were unable to reduce the images. The groups used in this study were first examined in 1995, after the first X-ray groups were discovered by Mulchaey et al. (1993). At the time, they were the only known groups observable from the southern hemisphere. We are looking at low-redshift groups since it has been only recently that the first samples of moderate-redshift galaxies have come out. The redshifts of the groups, which ranged from 0.006 to 0.025, were calculated spectroscopically in Zabludoff and Mulchaey (1998). These redshifts are averages for the entire group; however, since the brightest galaxy tends to sit in the middle of the gravitational potential its redshift is effectively the same as the group average (Zabludoff and Mulchaey, 1998). While we have the redshifts of group members to ensure that they are groups rather than superpositions of galaxies in the same field, these groups also have greater than five galaxies as an additional safeguard, as simulations suggest that many systems with fewer galaxies are in fact just superpositions.

The images were taken with XMM-Newton and are available for download through the NASA High Energy Astrophysics Science Archive Research Center

(HEASARC). XMM-Newton was used instead of Chandra because of the wider field of view (30′ on a side vs. 16.9′ on a side). The observation times for the groups varied from 7 – 42 ks. For information about the groups, see Table 1 and Table 2. Table 1 summarizes the characteristics of the XMM-Newton observations, such as coordinates, date, and XMM-Newton exposure time. This exposure time is the total number of seconds for the observation after removing any flaring events. Table 2 summarizes the observed group characteristics such as redshift and distance to the group. It also includes the number of kiloparsecs that correspond to a radius of 16′, which is approximately half the chip size of XMM-Newton.

Name	RA (J2000.0)	Dec (J2000.0)	Date	XMM ET (ks)
HCG 42	10h00m21.8s	−19d38m57s	2001-11-21	54.2
HCG 62	12h53m08.1s	−09d13m27s	2003-1-15	32.8
HCG 90	22h02m01.9s	−31d52m11s	2004-11-11	50.3
NGC 2563	08h20m35.7s	+21d04m04s	2001-10-15	58.9
NGC 4325	12h23m06.7s	+10d37m16s	2000-12-24	57.9
NGC 5129	13h24m10.0s	+13d58m35s	2000-07-07	49.6
NGC 533	01h25m31.3s	+01d45m33s	2002-12-31	110.0
NGC 5846	15h06m29.3s	+01d36m20s	2002-12-31	42.6
NGC 741	01h56m21.0s	+05d37m44s	2004-01-03	0.4

Table 1: A summary of the group properties, as well as the exposure times and dates. Coordinates refer to the center of the group. The XMM exposure time refers to the total livetime summed over the three detectors. The livetime is the exposure time after flaring events are removed.

A tiled image of all the groups in the optical band with X-ray contours is shown below in Figure 2.1. Figure 2.2 shows the reduced XMM-Newton images for each of the groups.

As explained §1.1, XMM-Newton has three detectors. Occasionally there would be a row of bad pixels in one of the detectors. This did not affect the reduction process.

Name	Redshift	Distance (Mpc)	$16'$ (kpc)
HCG 42	0.01277	53.7	243.2
HCG 62	0.01452	61.1	276.8
HCG 90	0.00848	35.5	163.2
NGC 2563	0.01592	67.1	302.4
NGC 4325	0.02538	107.7	476.8
NGC 5129	0.02332	98.8	440.0
NGC 533	0.01807	76.3	342.4
NGC 5846	0.00631	26.4	121.6
NGC 741	0.01853	78.3	350.4

Table 2: Physical properties of the groups. The last column corresponds to approximately half the chip size of XMM-Newton in units of distance.

Images taken using XMM-Newton can theoretically be reduced with any high-level analysis package used in high-energy astrophysics, but the Science Analysis Software (SAS) is best (Snowden et al., 2004). This software consists of approximately 125 programs and scripts for data reduction, extraction, and some analysis of XMM-Newton images. This package is not designed for higher-level scientific analysis such as spectral fitting and temporal analysis, but it can be used to reduce images and do preliminary spectral analysis (Snowden et al., 2004). [1]

2. The Reduction Process

2.1. Image Reduction. There are two types of files that are included in the downloaded data—ODF (Observation Data File) and PP (Pipeline Processing) files. To reduce the images, extensive calibration data is necessary, which must be available under a Current Calibration File (CCF) directory. The relevant information is included in a CCF Index File (CIF). Before starting the reduction process, the cshdef file must be edited to reflect the new directories, i.e. SAS_ODF and

[1]For more in-depth information, please refer to *The XMM-Newton ABC Guide: An Introduction to XMM-Newton Data Analysis*. All the steps in the reduction process described below can be found there, as well.

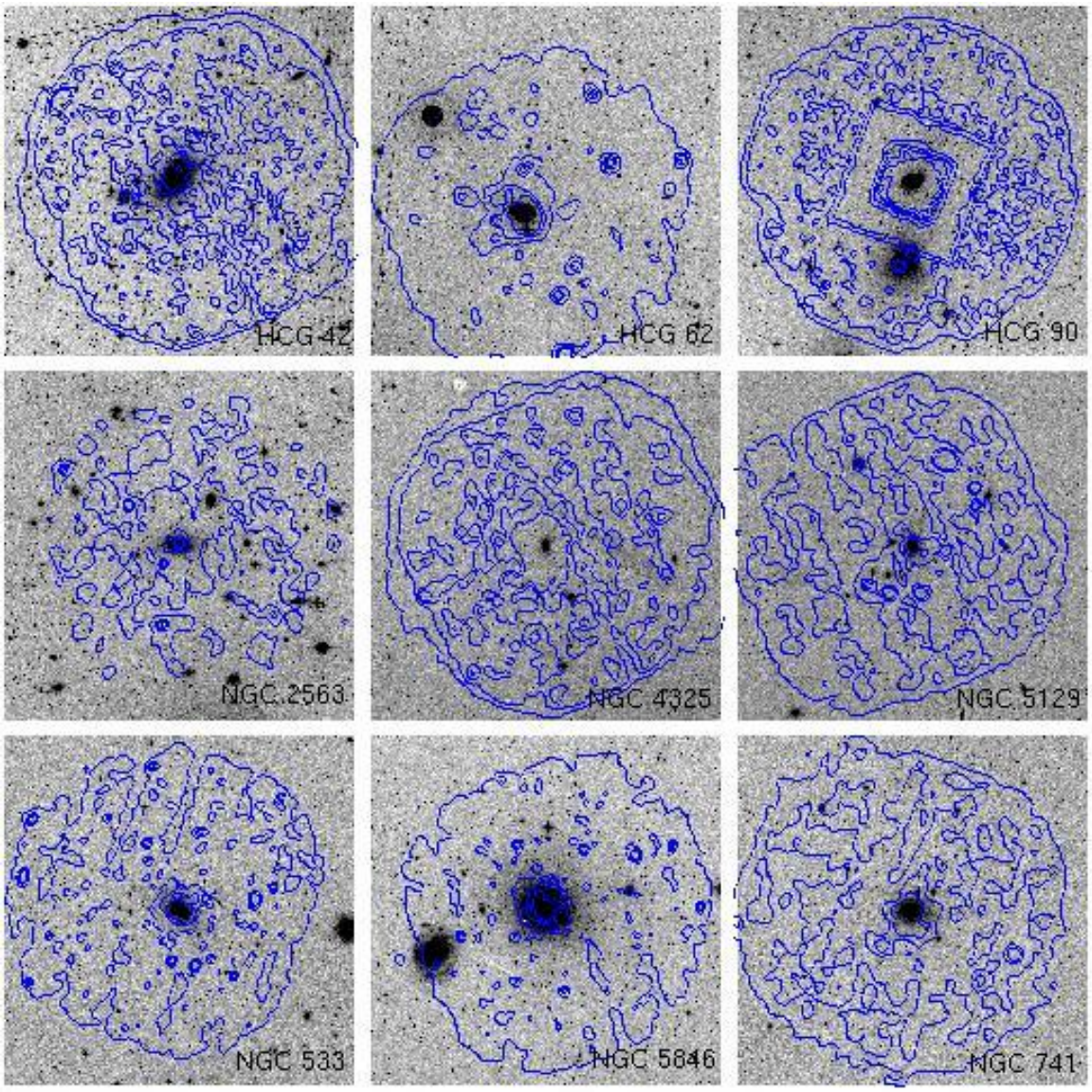

Figure 2.1: The nine groups used in this study. Images are taken from DSS-2 and are in the R band, and are overlaid with the X-ray contours from the XMM-Newton images. The DSS-2 images are 30′ on a side to match up with the XMM-Newton field of view.

SAS_CCF must be edited. In case the CCF has been changed, it is easiest to just recreate the CIF upon starting the reduction process. To reprocess the ODF data with the pipeline tasks, the ODF summary file must be extended, as well. This

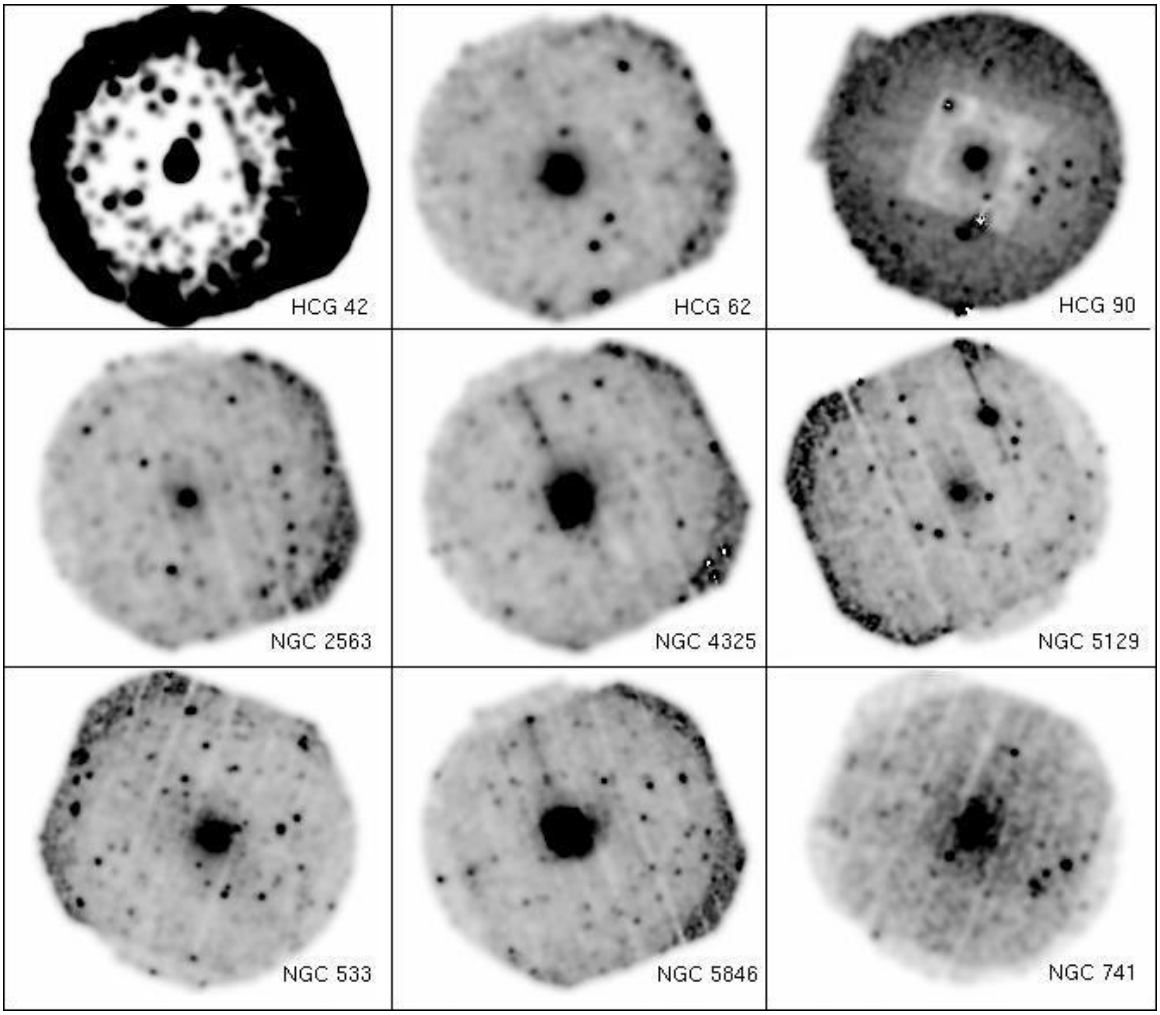

Figure 2.2: The nine groups used in this study, taken with XMM-Newton. The images from all three detectors have been coadded together. They are in the broadband (0.5 - 8 keV) range.

adds information extracted from the instrument housekeeping data files and the calibration database. Once this is done, the pipeline products can be produced.

Data from each of the three detectors should be processed separately, following the same routine for each one. The commands and parameters for this process were provided by Dr. John Mulchaey. First, a filtered event list should be created for the energy range 0.5 – 8 keV. This creates an output file that has much of the

contamination due to low-pulse height events removed. Once this event list has been created, the high-energy events (energy greater than 10 keV) are filtered out. When doing this, only single pixel events were selected. Here we tried to eliminate events due to flares, rather than events coming from the scientific target. Once the images were filtered, we made clean images, which were then used to create an exposure map. The exposure map is used to account for non-uniform coverage on the chip. To make the exposure maps, we created an attitude file using a time step of one second. Both of these were then used to detect the sources. The sources were then removed from the clean images to do additional flare removal.

In addition to making event files for the entire image, event files were made for both the soft (0.5 – 2 keV) and hard (2 – 8 keV) bands. Much of the emission in the soft band is likely due to the diffuse gas surrounding the group, so to look for point sources we only examined the sources in the hard band. We then detected sources in both the bands. The sources were saved in a list that included information such as the coordinates of the source, the number of photon counts for each source, and the flux of each source. Both the number of photon counts and the flux were provided for each of the detectors. The flux was converted to $erg/s \cdot cm^2$ assuming a "thin" filter, a power law with a photon index of 1.7 (which is standard for AGN), and a neutral hydrogen column density of $3 \times 10^{20} cm^{-3}$. The flux was then used to calculate the luminosity of each source. The luminosity calculation will be discussed further in §3.1.

We also made exposure maps for the total band, which we then normalized using the `imstat` and `imarith` tools in IRAF (Image Reduction and Analysis Facility). This was done separately for all three of the detectors, and the three images were then mosaiced together and smoothed. Figure 2.3 below shows both an unprocessed and a processed image.

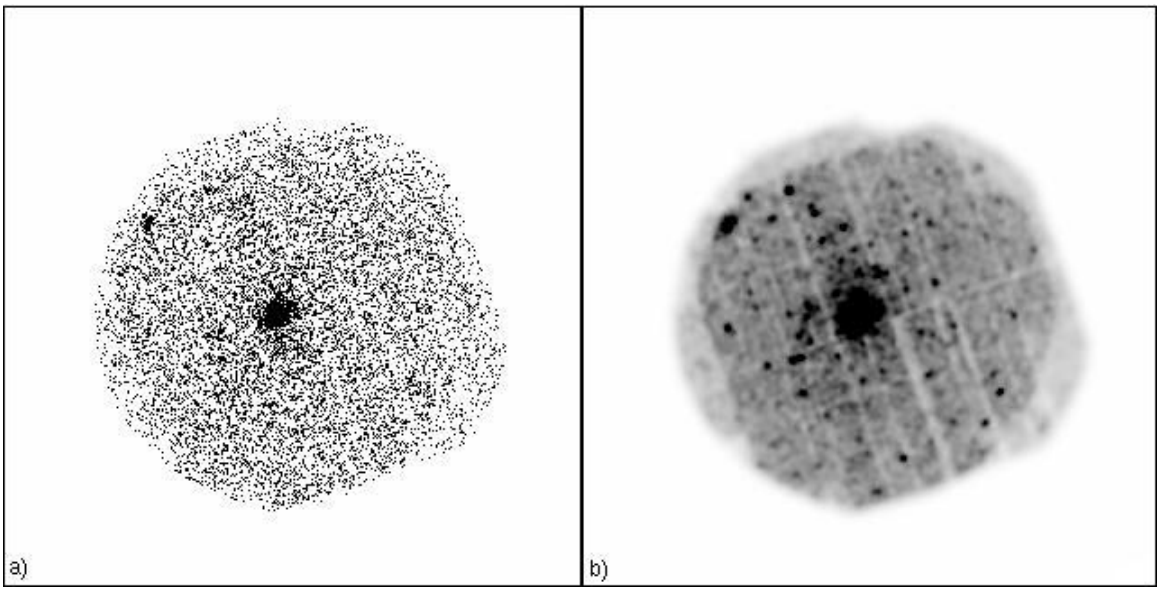

Figure 2.3: Side by side comparison of a raw (panel a) image and a processed (panel b) image for the group HCG 42, for all three detectors mosaiced together. The processed version does not include the exposure map.

These X-ray images were used to make X-ray contour maps, which were then overlaid on images from the *SkyView* Digital Sky Survey (DSS).

2.2. Spectral Fitting. Because XMM-Newton also has spectrometers, it is possible to extract spectra from the sources in the processed images. While the above steps were carried out from the command line, it is easier to extract spectra using the SAS GUI. To do this, we ran `xmmselect` on the final event file for each group. This provides a ds9 window with the image displayed, from which we chose the source of interest and extracted a spectrum. It is also necessary to extract a spectrum from the background. Next we created the photon redistribution matrix (RMF), which corrects for the distribution of the photons on the detector, and the ancillary response file (ARF), which corrects for the location of the source on the detector.

Once the spectrum was extracted, it needed to be prepared for fitting using the `FTOOLS` task `grppha`. To do this we included the background spectrum, the RMF, and the ARF. We also binned the data so there would be 25 counts in each bin.

The spectra were fit using *Xspec*. We used two different models on the sources—an absorbed power law and an absorbed thermal emission model. We ignored data that was outside of the 0.5 – 8 keV band. The galactic absorption column density was set to 10^{20} cm^{-3}. For the power law the index was set to 1.7, which, as mentioned above, is the standard value for an AGN. We used the default normalization model. For the thermal emission model, we set kT to one and the metal abundance to 0.5 and accepted the default option for the other parameters.

CHAPTER 3

Data Analysis

1. Catalogs

1.1. The X-ray Catalog. As mentioned in §2.2, a list of the X-ray point sources was created during the reduction process. This list was the starting point for determining which sources were AGN. It included the Right Ascension and Declination (J2000.0) of each point, as well as the number of counts and flux for each detector. From this list we were able to create a list of X-ray point sources, and narrow that down to sources that belonged to one of the groups of interest. Figure 3.2 is an organizational tree that more clearly depicts the creation of the X-ray catalogs.

The redshifts of each source were found using the coordinates extracted from SAS and doing a near-object search with the NASA Extragalactic Database (NED). The initial search radius was determined assuming XMM-Newton has a pointing error of two arcminutes, which is quite generous. Figure 3.1, however, shows that the offset between XMM-Newton and NED is significantly smaller. Because of this, we decided to use only those objects within $0.25'$, which corresponds to $15''$. The list of point sources from XMM-Newton was divided into three groups—a group with redshifts belonging to one of the groups, a group with redshifts outside of the group, and a group with no redshifts. For an object to be considered a group member, its velocity had to be within $\pm$ 3,000 km/s of the group's. The

redshift for each group was determined through spectroscopic observations done by Dr. Zabludoff and Mulchaey (1998). This is discussed in greater detail in §2.1.

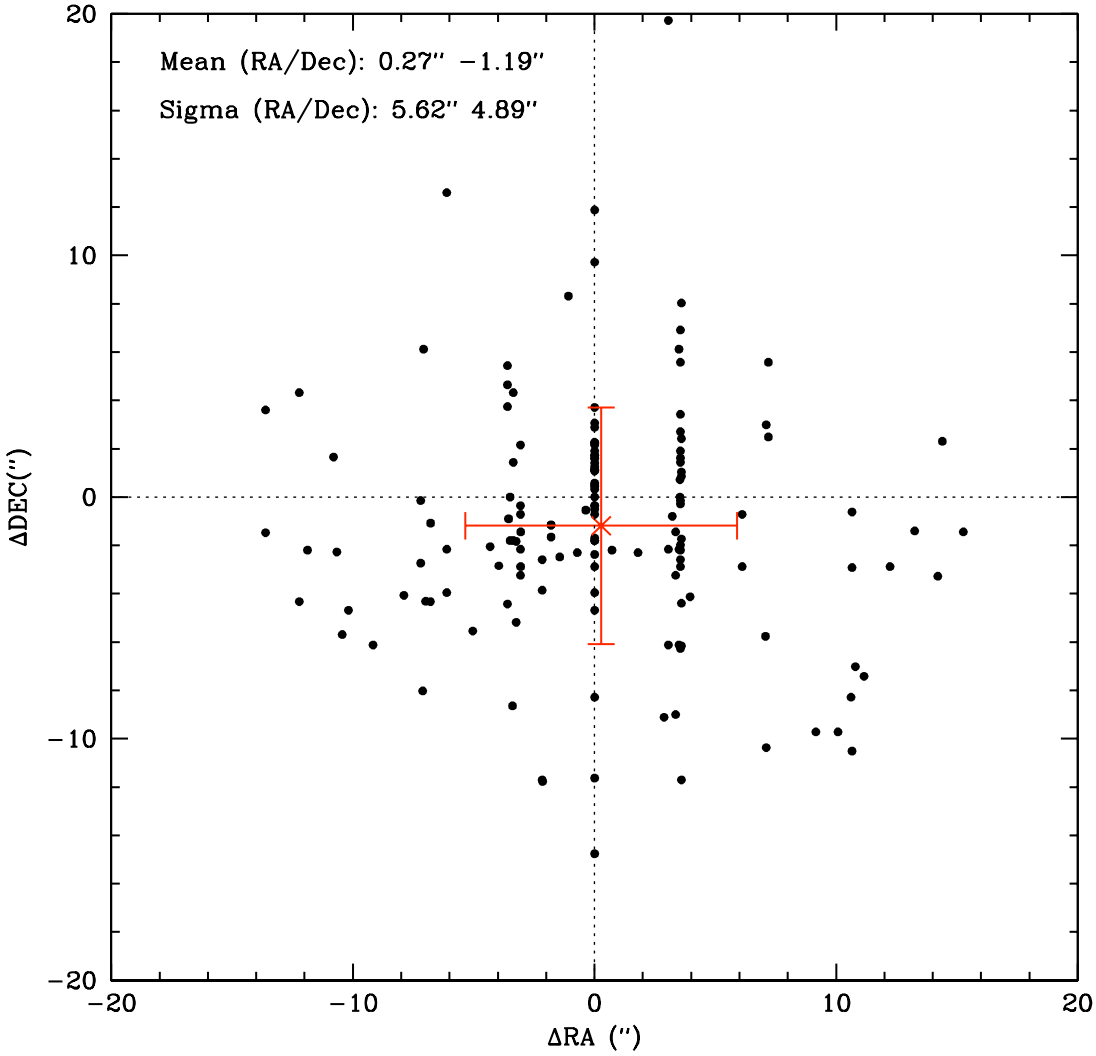

Figure 3.1: The astrometric offset between XMM-Newton and NED. This was used to limit the search radius around each point source when looking for an optical counterpart. The binning seen here is due to rounding in the XMM-Newton coordinates. The red x marks the mean offset in RA and DEC. The plotted error bars correspond to ± one standard deviation.

Occasionally more than one X-ray source mapped to the same optical source. When this happened, one of the sources was thrown out. This is why there are fewer sources in the clean catalog than in the catalog that included every point source extracted that belonged to a group, as seen in Figure 3.2. Because of the algorithm SAS uses to extract point sources, some of the point sources are actually X-ray emission from the same optical source. This is more likely to happen with extended sources, and will be discussed in greater detail below.

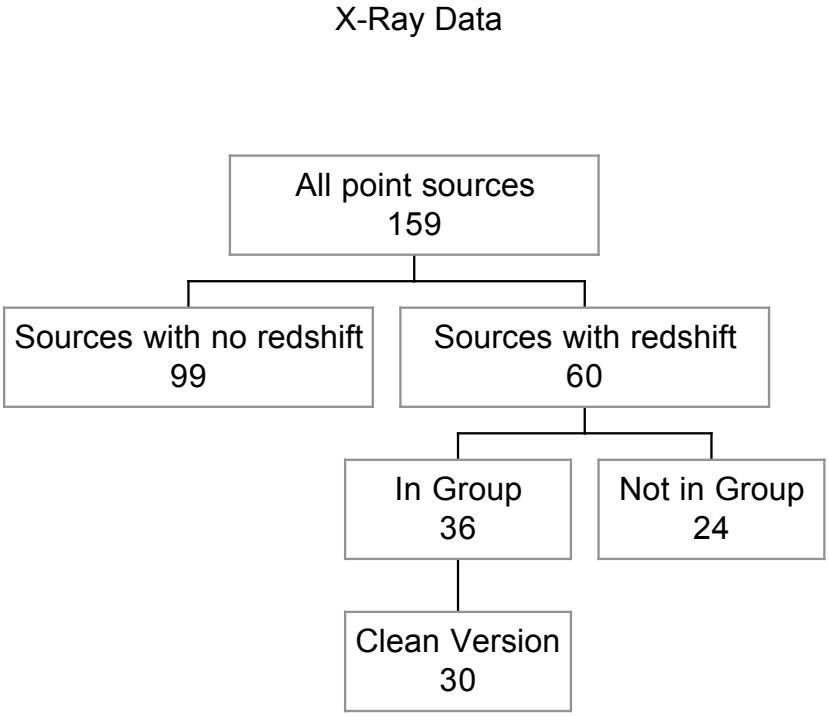

Figure 3.2: A visual representation of the filtering done on the X-ray sample. If an X-ray source belonging to one of the groups yielded more than one object with the same coordinates in NED, only the one closest to the center was kept. Those sources made up the clean sample.

Figure 3.3 shows the distribution of the redshifts among the sources. It illustrates that the majority of X-ray detections could not be identified by redshift. It also shows the population of sources that did not belong to a group. Although a majority of the X-ray sources did not have redshfits noted in NED, based on the central concentration of sources shown in Figure 3.4 we have reason to believe that some of these sources are group members. it is also likely that many of these X-ray detections are from the intra-group medium (i.e. the hot diffuse gas associated with the group). This implies that the number of total group members is higher than what we have found here. Some of these sources could indeed be AGN, which could potentially change our calculated AGN fraction. Figure 3.5 shows the redshift distributions of the confirmed group members once the contaminants were removed.

In addition to redshifts and coordinates, NED also includes information on what kind of source the object is. If the source was purely an X-ray source with no counterpart in any other wavelength it was thrown out. Using the X-ray flux extracted during the reduction process, one can find the X-ray luminosity of the object using the luminosity equation,

$$L = 4\pi f d^2, \tag{3.1}$$

where f is the flux of the object and d is the distance to the object. This was done only for objects with redshifts. Only those objects belonging to a group were analyzed in any detail, as they were the only objects of interest for this study.

1.2. The Optical Population. Once the catalog of X-ray sources was created, it was necessary to create a list of optical galaxies in each group. To do this, we needed information from both the point source catalog in the Two Micron All

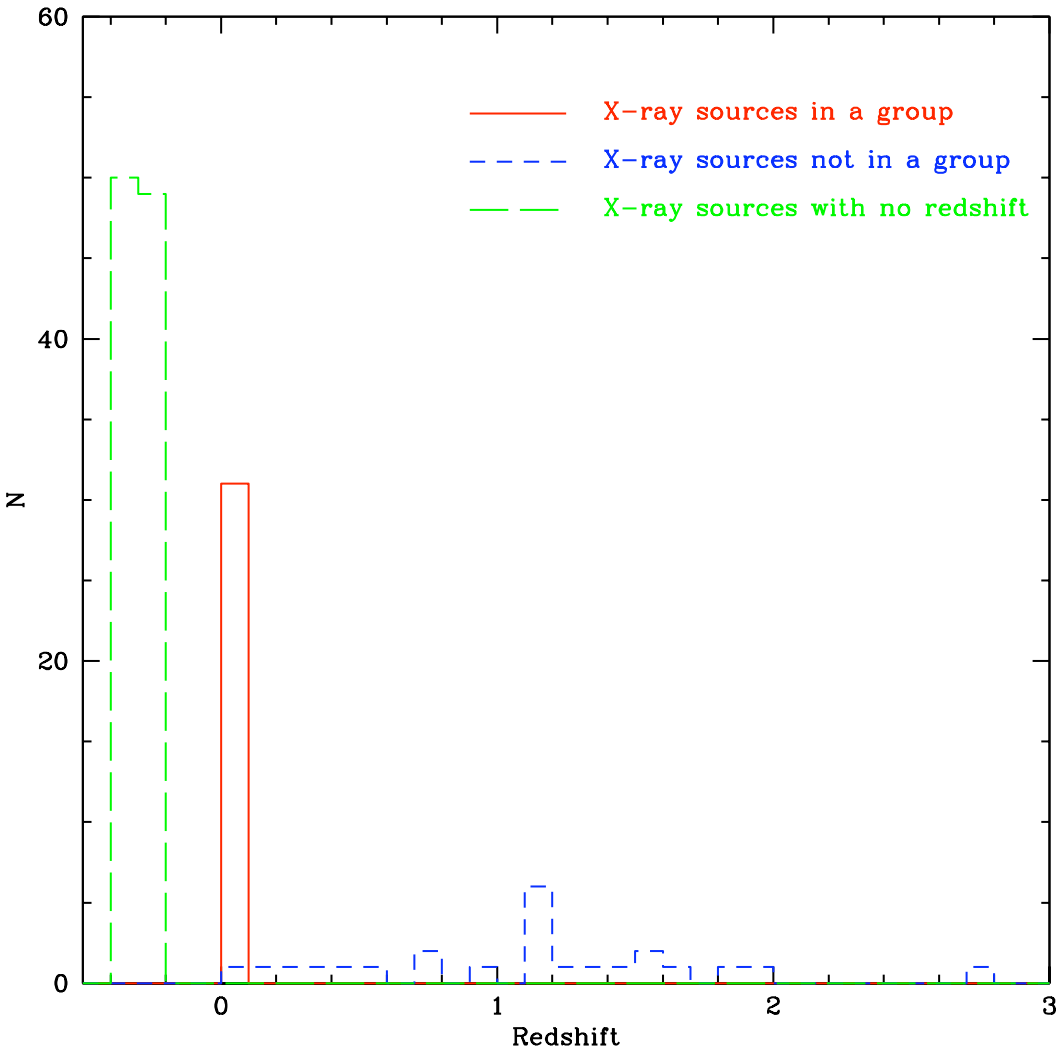

Figure 3.3: The redshift distribution for all the point sources from the X-ray images. Point sources with no available redshift were arbitrarily assigned $z = -0.2$ or $z = -0.3$ for visualization purposes.

Sky Survey (2MASS) in the near infrared (NIR) and NED. 2MASS has scanned the entire sky searching for point sources, and is a joint endeavor between the University of Massachusetts and the Infrared Processing and Analysis Center (IPAC).

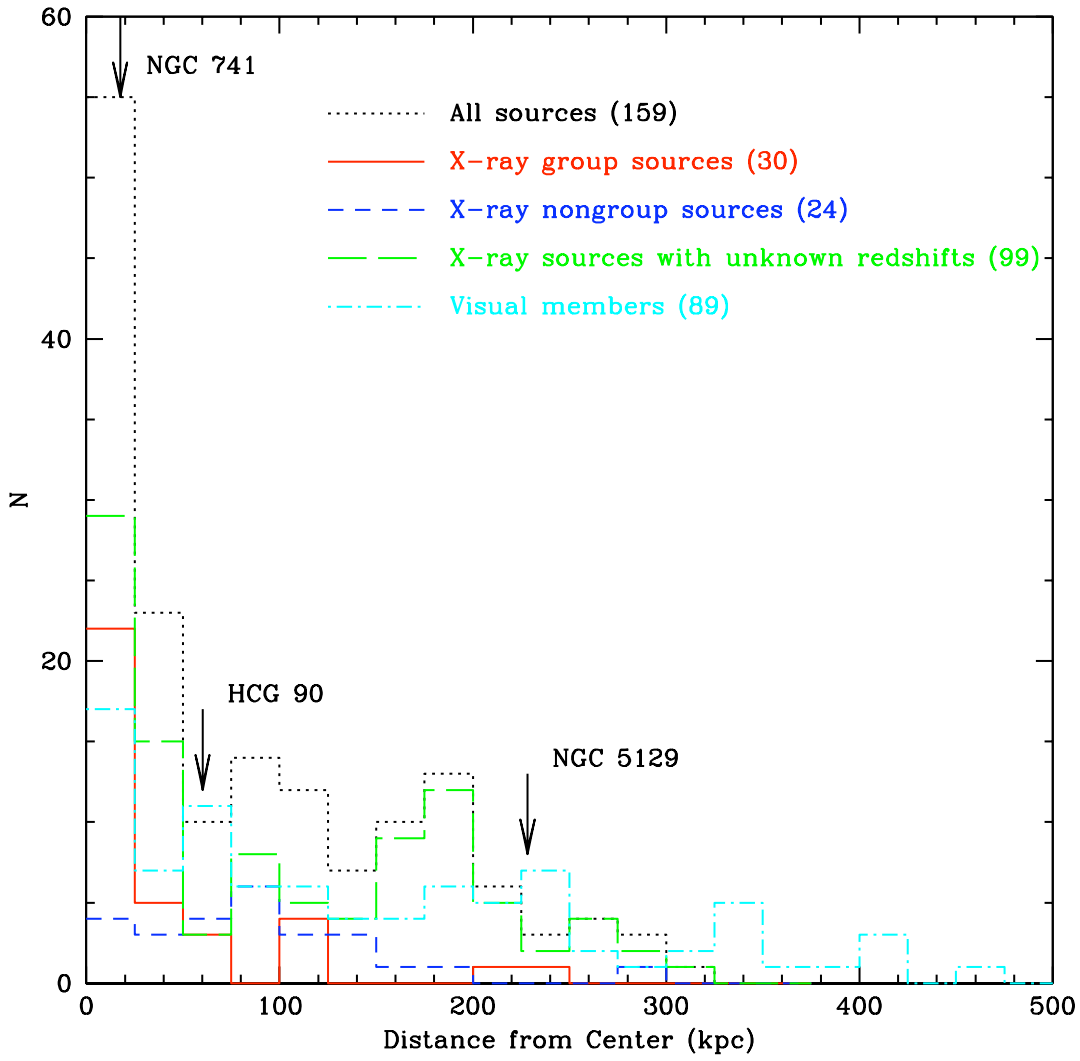

Figure 3.4: The distribution of point sources from the center of the group, with the group members from the optical catalog shown in aqua. The majority of X-ray sources are most likely detections of the intragroup medium eminating from the center of the group, which is why many of the sources are clustered within 20 kpc of the group center. The AGN are marked with arrows.

The limiting magnitude for the 2MASS point source catalog is 15.8 for the J band,

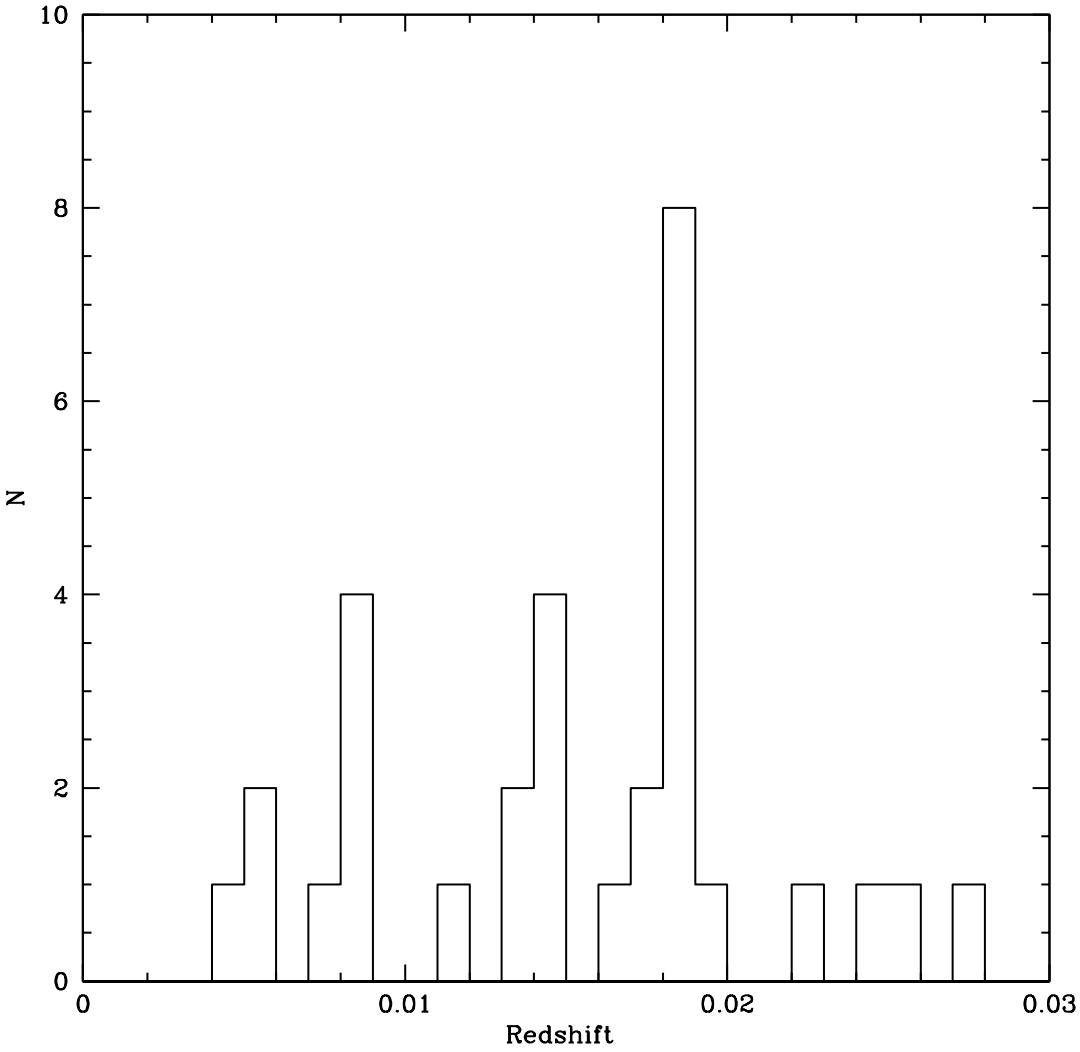

Figure 3.5: The redshift distribution for X-ray point sources that are members of one of the nine groups.

15.1 for the H band, and 14.3 for the K_s band (Skrutskie et al., 2006). Figure 3.6 shows what each of the existing catalogs was used for.

These optical group members were found using a near name search of each galaxy in NED. The search radius was 16 arcminutes, which is approximately the

size of the XMM-Newton field of view. The redshift was constrained within ±0.001 of the group's redshift to select for galaxies in the group. Only objects that were listed as galaxies in NED were considered for this catalog.

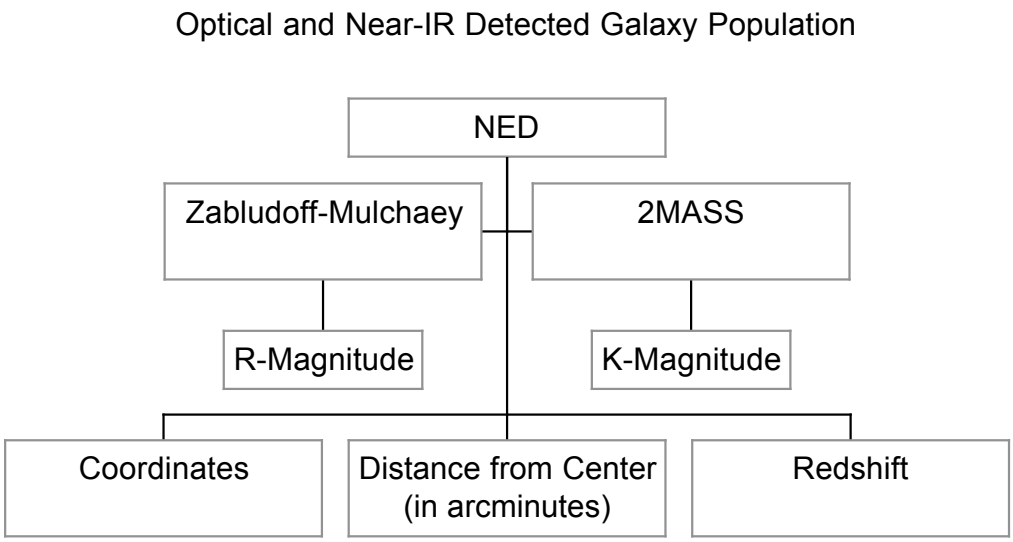

Figure 3.6: A visual representation of the different catalogs used to create the list of optical galaxies in the groups, as well as the information needed from each catalog.

Because we made a magnitude cut, it was necessary to get the absolute R magnitude (M_R) of the optical sources. Five of these groups were included in the Zabludoff-Mulchaey Catalog, which is part of a larger spectroscopic survey of the properties of poor galaxy groups (Zabludoff and Mulchaey, 1998). They have published the apparent R magnitudes (m_R) of many of the galaxies in the catalog

of optical counterparts to the X-ray sources. These apparent magnitudes could then be used to calculate M_R. When m_R was not available, we found the apparent K band (2.2 μm, in the infrared region) magnitude (m_K) from 2MASS and used it to calculate the absolute K magnitude (M_K). The majority of galaxies missing M_R information were not in the Zabludoff-Mulchaey catalog, although a few may have been too faint to have been included. M_K was obtained for all sources, and the relationship between the two magnitudes was calculated by finding the line of best fit for a simple M_R v. M_K scatterplot, which can be seen in Figure 3.7. When no R magnitude was available, it was calculated from that relationship. This optical catalog includes 89 sources, although not all 89 had available magnitudes in any band.

1.3. Merged X-ray and Optical Catalog. When the X-ray data was combined with the optical catalog we were able to determine the AGN fraction. Using the X-ray source's position and redshift we were able to compare the two catalogs and match the X-ray sources with the visual sources to create a combined catalog. From the X-ray catalog we determined the number of AGN in the sample and then used the optical catalog to determine the total number of galaxies in the groups. The actual calculation will be described in §4.3.

2. X-Ray AGN Diagnostic

For an object to be considered an AGN, it had to be a point source with an X-ray luminosity greater than $L_X = 10^{41}$ erg/s in any one of the three detectors. This luminosity was chosen because it is high enough that anything above it should be an AGN, ensuring that the source's emission is not because it is a low-mass X-ray binary or that it is from the hot X-ray gas surrounding the group. We are only using one of the detectors to set the cutoff because of the low number of

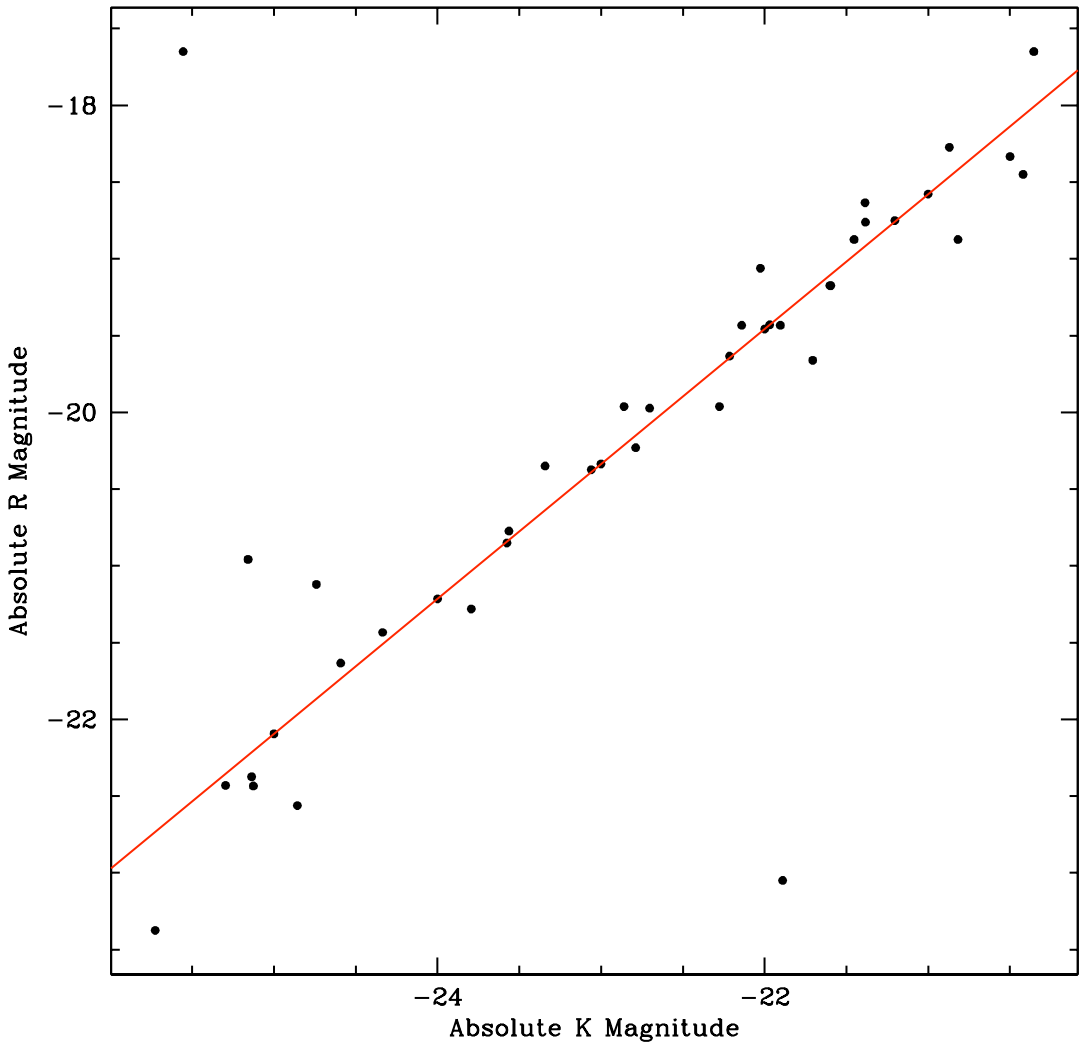

Figure 3.7: Absolute K magnitudes from 2MASS plotted against absolute R magnitudes from the Zabludoff-Mulchaey catalog. The resulting relationship was used to calculate the absolute R magnitude when only the K magnitude was available: $M_R = 0.8791 M_K - 0.1161$.

photon counts that hit the detectors. The large spread in luminosities for each detector seen in some of the sources can also be attributed to the low number of counts associated with X-ray astronomy. This luminosity was chosen so that

the AGN fraction of this survey could be more meaningfully compared to that of other surveys. The contour overlays described in §2.2 helped visualize the different X-ray sources. These can be seen in Figure 3.8. The AGN in HCG 90 and NGC 741 had high X-ray luminosities which is reflected in these contours. The contours for the central galaxy of a group also show large amounts of X-ray emission. All of the contours displayed, with the exception of the AGN, are set to the same pixel scale. The AGN were done on separate scales to show the contours more clearly.

3. SAS Reduction Algorithm

Although there were 30 X-ray point sources, there are only 21 contour overlays. Although not immediately obvious when comparing the X-ray coordinates with the coordinates from NED, it became clear when creating the contour overlays. Many of the optical images from DSS were of the same object. This raises the question of how to handle these sources. There are two potential approaches one could take—assume that the duplicates are all from the same source and add their fluxes, or treat them as separate sources and consider their fluxes individually.

We have chosen to take the latter approach. A source is most likely going to be broken up into many point source detections if it is an extended source. This is most likely the case with our duplicate sources. The four groups where this occurred are HCG 62, HCG 90, NGC 533, and NGC 741. It did not affect any of the sources we designated as AGN. In all three groups, it was the X-ray detection from the central galaxy that got split into multiple detections. The diffuse X-ray gas is centered on these galaxies, so despite removing detections from the soft X-ray band (0.5 – 2 keV) and using only detections from the hard band (2 – 8 keV) there were likely enough photons emanating from the source to be detected in the

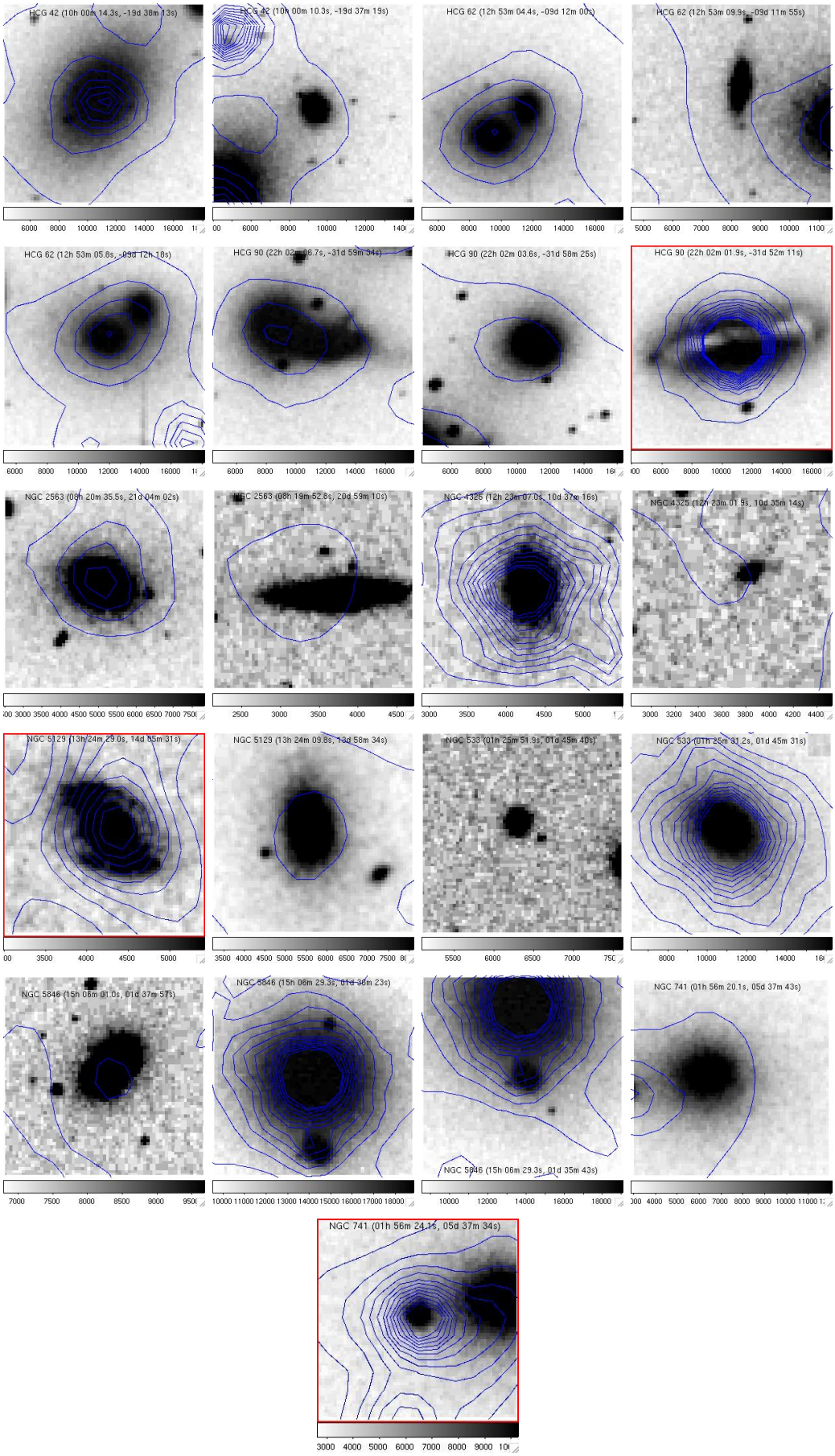

Figure 3.8: The X-ray contours are shown overlaid on top of optical images from the Digital Sky Survey. Each image is 0.03′ on a side. The AGN are surrounded by a red box. Duplicate sources have been removed.

hard band. Thus adding the fluxes could cause a source to be counted as an AGN when really it just has a large amount of diffuse X-ray gas surrounding it.

CHAPTER 4

Results and Discussion

1. Results

Using a lower limit of $L_X = 10^{41} erg/s$, we found a total of three AGN, each of which exceeded that limit in at least one of the three detectors. Figure 4.1 shows the X-ray luminosity for each of the point sources belonging to a group. These AGN are in HCG 90 (NCG 7172, 22h 02m 03.2s, −31d 59m 11s), NGC 5129 (NGC 5132, 13h 24m 29.0s, 14d 05m, 31s), and NGC 741 (NGC 742, 01h 56m 24.2s, 05d 37m 36s). Although there is an X-ray point source in the group NGC 4325 that qualifies as an AGN based on our selection criteria, its high X-ray luminosity is most likely due to the X-ray emission of the intragroup medium, since the galaxy sits at the center of the group. This will be examined in more detail in §4.2.

Figure 4.1 shows that two of the AGN have average X-ray luminosities below the minimum cutoff. When calculating the averages negative values were not included. As discussed in §3.2, we only used the X-ray luminosity calculated from one detector, as the low number of photon counts hinder our ability to get a good average. Thus, since each of these two had at least one X-ray luminosity greater than $L_X = 10^{41}$, we considered them to be AGN. Additionally, examining the spectra provides further confirmation that these are, in fact, AGN. Applying both a power law and a thermal emission model to the data shows that the power law is the better fit, which is characteristic of an AGN.

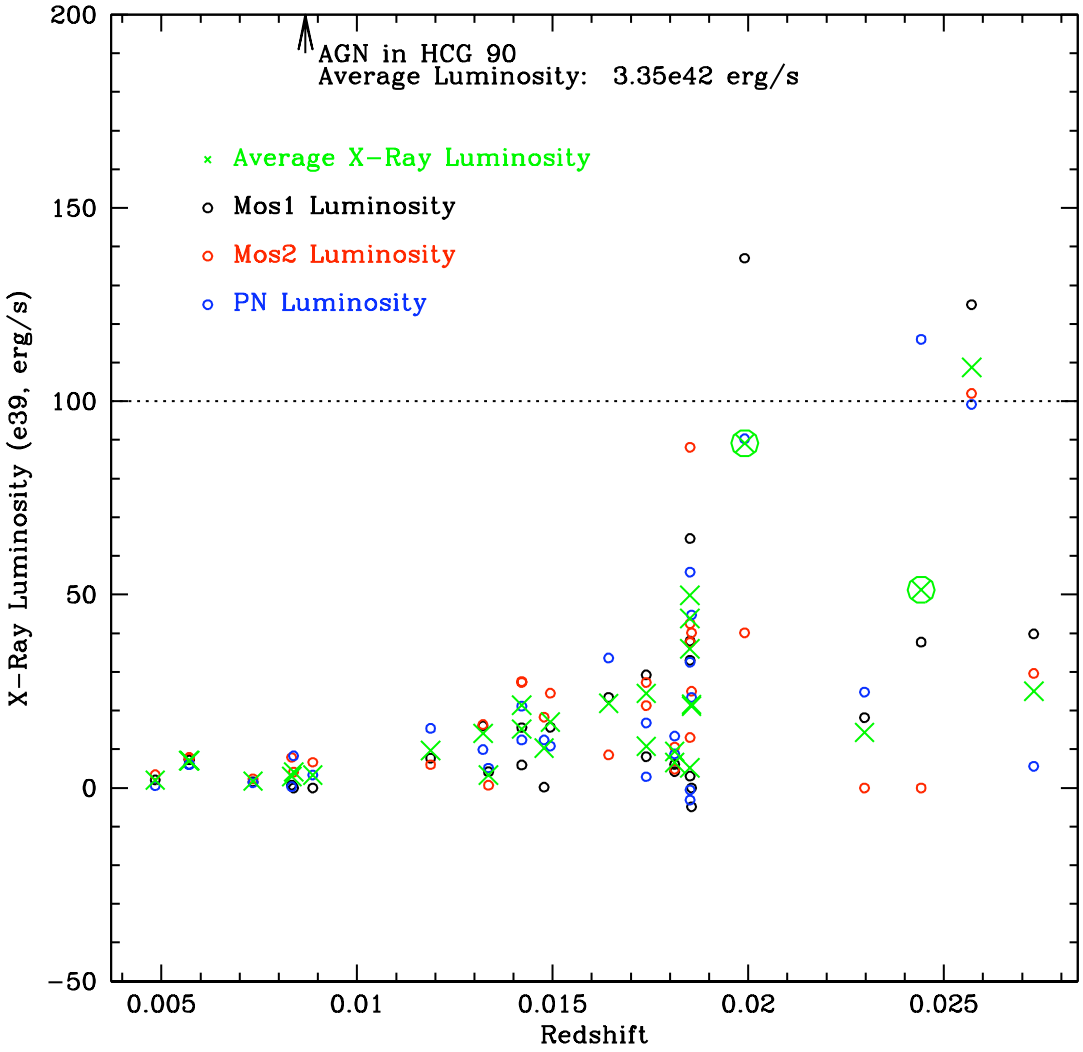

Figure 4.1: The X-ray luminosity plotted against the redshift of the galaxy. The dashed line represents the lower luminosity limit for an AGN. The AGN are circled. If there were problems with a detector such as a negative luminosity, it was left out of the average. For scale issues, the AGN in HCG 90 is not shown, but is marked with an arrow. The source with L_X above the lower luminosity limit but not circled belongs to the group NGC 4325. We are not considering it to be an AGN because it is the central galaxy and the X-ray emission is most likely due to the large amounts of diffuse X-ray gas associated with it.

2. NGC 4325

One of the most notable things about Figure 4.1 is that one of the sources in NGC 4325 ($z = 0.02538$) has an X-ray luminosity above the minimum cutoff for an AGN, yet we are not classifying it as such. This particular galaxy is NGC 4325 (12h 23m 06.7s, 10d 37m 16s). It is the central galaxy in the group, and as such has a large amount of hot X-ray gas emanating from that particular location. It also is very bright optically, as seen in Figure 4.2. This is consistent with the idea that the peak of the X-ray emission generally coincides with a luminous elliptical or S0 galaxy that also tends to be the most luminous group member (Zabludoff and Mulchaey, 1998). The X-ray contours do not have the appearance of a point source, either, which further supports the idea that this galaxy is not a current AGN.

Additionally, this group is radio-quiet, which indicates that it is not currently active (Russell et al., 2007). Recent investigation of this group by Russell et al. (2007) used Chandra and found that there are two cavities in the intragroup medium (IGM). These cavities suggest that there may have been an outburst recently, although because there is no radio emission this outburst must have occurred long enough ago for the radio lobes to have faded. They propose that this outburst occurred between 10^7 and 10^8 years ago, which is the typical timescale to clear out a radio lobe (Carroll and Ostlie, 2007). They also found that the group has a steep entropy profile, which suggests that the group has been able to cool rapidly after a small AGN outburst. From the short cooling period of the gas, it can be inferred that the group is most likely in a pre-outburst stage. It is unknown whether weak outbursts are typical of this system or whether the most recent outburst was particularly weak, setting the stage for a much larger outburst (Russell

et al., 2007). It is possible that AGN experience several episodes of activity during the host galaxy's history as it undergoes mergers and encounters other sources of fuel (Carroll and Ostlie, 2007)).

3. Calculating the AGN Fraction

The AGN fraction (f_A) is defined as follows:

$$f_A = \frac{N_A}{N_{tot}}, \tag{4.1}$$

where N_A is the total number of AGN in the sample and N_{tot} is the total number of group galaxies.

We calculated f_A for three different scenarios:

(1) f_A including all the optical galaxies in the groups,

(2) f_A using an optical magnitude cutoff, $M_R < -20$,

(3) and f_A using the magnitude cutoff as above, as well as a radius cutoff of 250 kpc.

With no restraints imposed, there were a total of 89 galaxies, which gave us $f_A = 3.4^{+4.1}_{-2.1}\%$. The selection criteria for these galaxies is discussed in §3.1. The majority of the optical group sources, however, had magnitudes greater than $M_R = -20$. Taking this into account, the total number of galaxies is reduced to 27, and $f_A = 11.1^{+13.6}_{-7.0}\%$. This limit was chosen so that we would be able to compare our results to those of other surveys, especially Martini's. Their limit was set by the spectroscopic completeness of their observations of the more distance clusters (Martini et al., 2006). In addition to this magnitude limit, we also imposed a radius cutoff of 250 kpc so that each group would be probed to the same physical volume, although this is not entirely true as the closer groups were smaller than 250 kpc in size. Table 1 shows how large each XMM-Newton field of view is

in physical size for each group. Figure 4.3 shows the distribution of the different sources in each catalog, as well as the location of the AGN. The group members are circled in red, the sources with redshifts outside of the groups are circled in blue, sources with unknown redshifts are circled in green, and the optical galaxies of the group are circled in aqua. To avoid crowding, duplicate sources are not shown, and if the optical galaxy had an X-ray counterpart, only the X-ray counterpart is shown. The large black circle shows the 250 kpc radius for each group. There is also a smaller magenta circle with a radius of 125 kpc so that the closer groups can be compared with those that are further away. This inner circle is only for comparison purposes and was not used anywhere else in this study. The groups are shown separately. With this final constraint, the catalog of optical galaxies decreased to 24, and the AGN fraction increased slightly to $f_A = 12.5^{+15.3}_{-7.9}\%$. All of these uncertainties correspond to 90% single-sided confidence limits calculated by Poisson statistics (Gehrels, 1986).

4. Comparison to Other Surveys

Examining the AGN fraction of galaxy clusters, Martini et al. (2006) found that $f_A(M_R < -20) = 5 \pm 1.5\%$, which was five times higher than previously thought. Their sample consisted of eight low-redshift ($0.05 < z < 0.31$) clusters containing between two and ten X-ray sources per cluster, with a total of 40 X-ray sources. It was chosen because each of the clusters has publicly available Chandra data with sufficiently long exposure times. These clusters are also all observable from the Las Campañas Observatory in Chile, where they obtained their visible-wavelength spectroscopic data (Martini et al., 2006). This is comparable to the number for the groups presented here, which have between two and eight X-ray sources. We found a total of 30 X-ray sources spread over the nine groups. They

conservatively estimate (based on the lower X-ray luminosity limit) that 35 of their X-ray sources are AGN, although only a small fraction of these AGN would be classified as such based upon their visible-wavelength spectra. Here we find that for groups, $f_A(M_R < -20) = 11.1^{+13.6}_{-7.0}\%$, using the same X-ray luminosity cutoff ($L_X = 10^{41}$ erg/s). Their value falls within the range set by our single-sided lower confidence limit.

Our results somewhat contradict results recently published by Shen et al. (2007)), who found that among low redshift galaxy groups ($z \sim 0.06$) all but one of their AGN population were identified by their optical emission lines. The X-ray detected AGN is a member of the only X-ray luminous group in their sample. They found six AGN out of approximately 140 galaxies, giving them a calculated AGN fraction is $\sim 7\%$, which is also within our uncertainty limits. This number is complete to $M_R = -20$.

The difference between their study and that of Martini's was in the population of AGN, rather than AGN fraction. Martini's sample had a larger X-ray bright AGN population but not many optically-selected AGN. They hypothesize that these two populations are in fact the same population of super-massive black hole, just at different epochs. The AGN in groups are in the high-accretion optically dominant phase, which is earlier in their evolution, while those in the clusters, which are more evolved systems, are in the low-accretion X-ray dominant phase (Shen et al., 2007).

Our AGN fraction is slightly higher, however all of our AGN were X-ray detected. This difference could be due to a difference in sample type. All of our galaxies were X-ray luminous, while only one of Shen's was, which is where they found their X-ray luminous AGN. These X-ray luminous groups can be thought

of as "mini-clusters" (Mulchaey, 2000), so it is not too much of a stretch to anticipate finding X-ray luminous AGN. These two results could potentially help us to understand the role that host galaxy environments play in regard to the fueling and evolution of AGN.

5. Future Work

All of the groups in this sample are visible from the southern hemisphere, which is where Las Campañas, the telescope operated by the Carnegie Observatories, is located. Thus, in the future, there is the potential to compare our results with spectroscopic results of these groups and see whether or not the AGN found here also have the characteristic optical spectra of AGN. In addition to the AGN population of groups, we can also examine the galaxy morphologies of these groups to help understand what determines their differences. We would also like to do a more rigorous comparison to the clusters to see if the difference in results is significant.

As mentioned in §3.1.1, it is possible that some of the sources without published redshifts could be members of a group. A statistical analysis could be done on these sources to find an upper limit on the AGN fraction by assuming that they are all group members and determining how many of those sources would exceed our luminosity cutoff. It is likely that the sources furthest from the center of the group would not be part of the group. The sources concentrated near the center of the field could either be associated with galaxies in the group or with the intra-group medium. If they were associated with the intra-group medium they would not have an optical counterpart and could be discarded.

It is also important to explore AGN in a variety of different environments. Already there are studies examining low-redshift clusters, and in this study we

look at low-redshift groups. We would like to explore the AGN fraction (as well as the characteristics above) at different redshifts. It appears that many galaxies encountered the group environment at $z \sim 2 - 3$, although it is hard to identify higher-redshift groups because of their sparse populations.

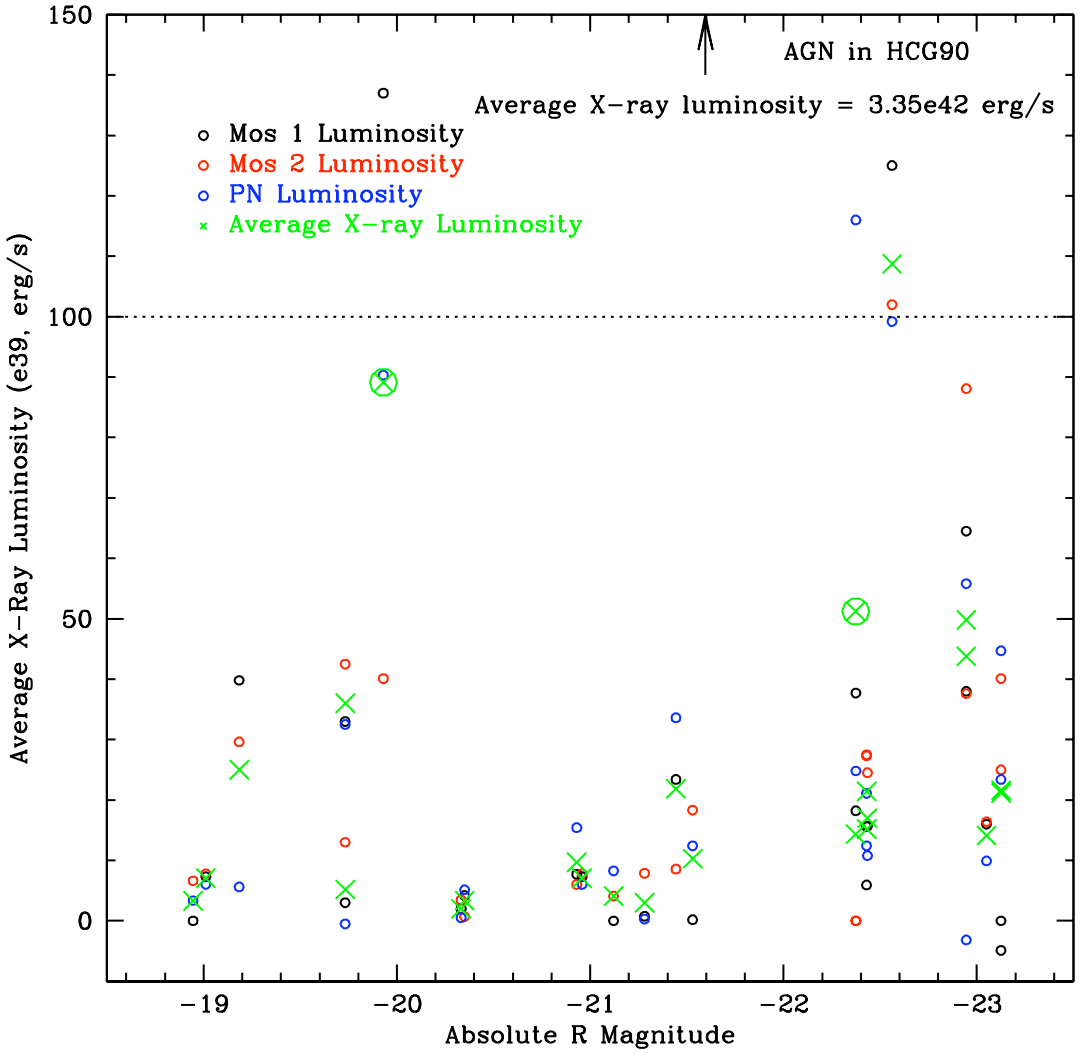

Figure 4.2: The X-ray luminosity of the group members plotted against the absolute R magnitude of the visual counterpart. The AGN are circled in green.

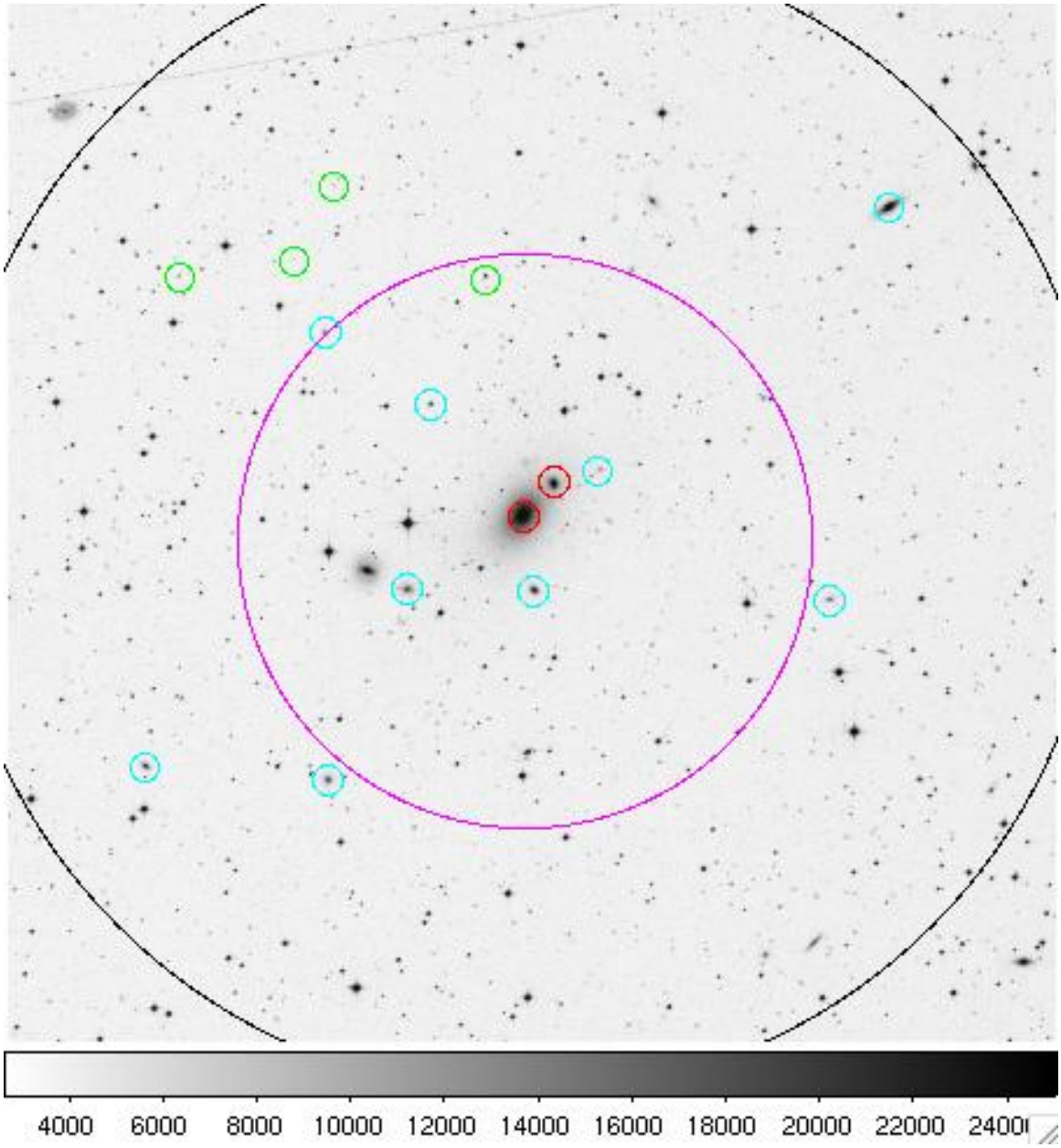

Figure 4.3: The distribution of X-ray sources and the optical galaxies in HCG 42. The images are R-band images from DSS-2. X-ray sources belonging to a group are circled in red, X-ray sources with redshifts outside of the group are circled in blue, X-ray sources with no known redshift are circled in green, and the optical galaxies are circled in aqua. The large black circle has a radius of 250 kpc. For reference, the magenta circle has a radius of 125 kpc. These conventions are held throughout.

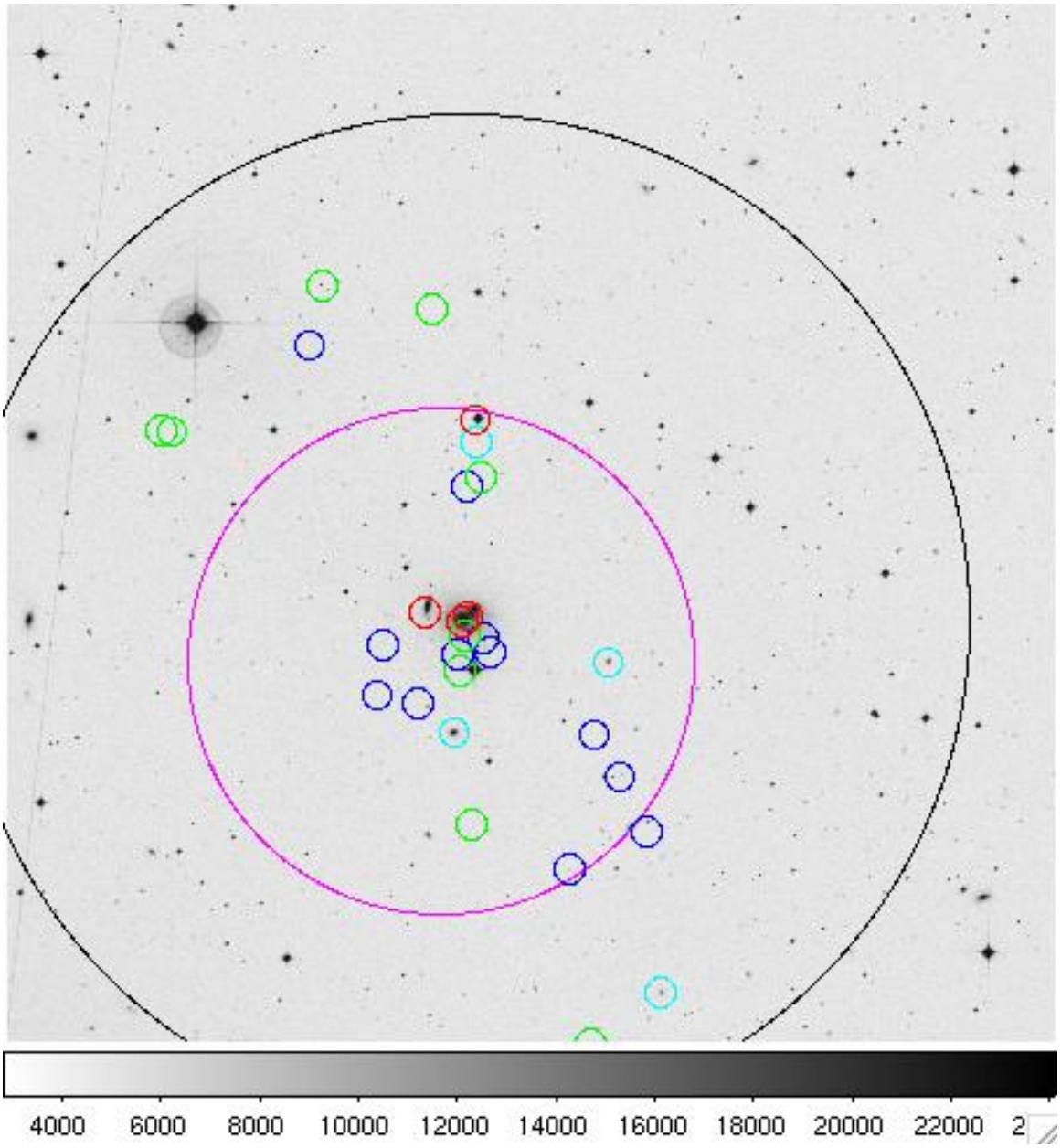

Figure 4.3: The distribution of X-ray sources and the optical galaxies in HCG 62.

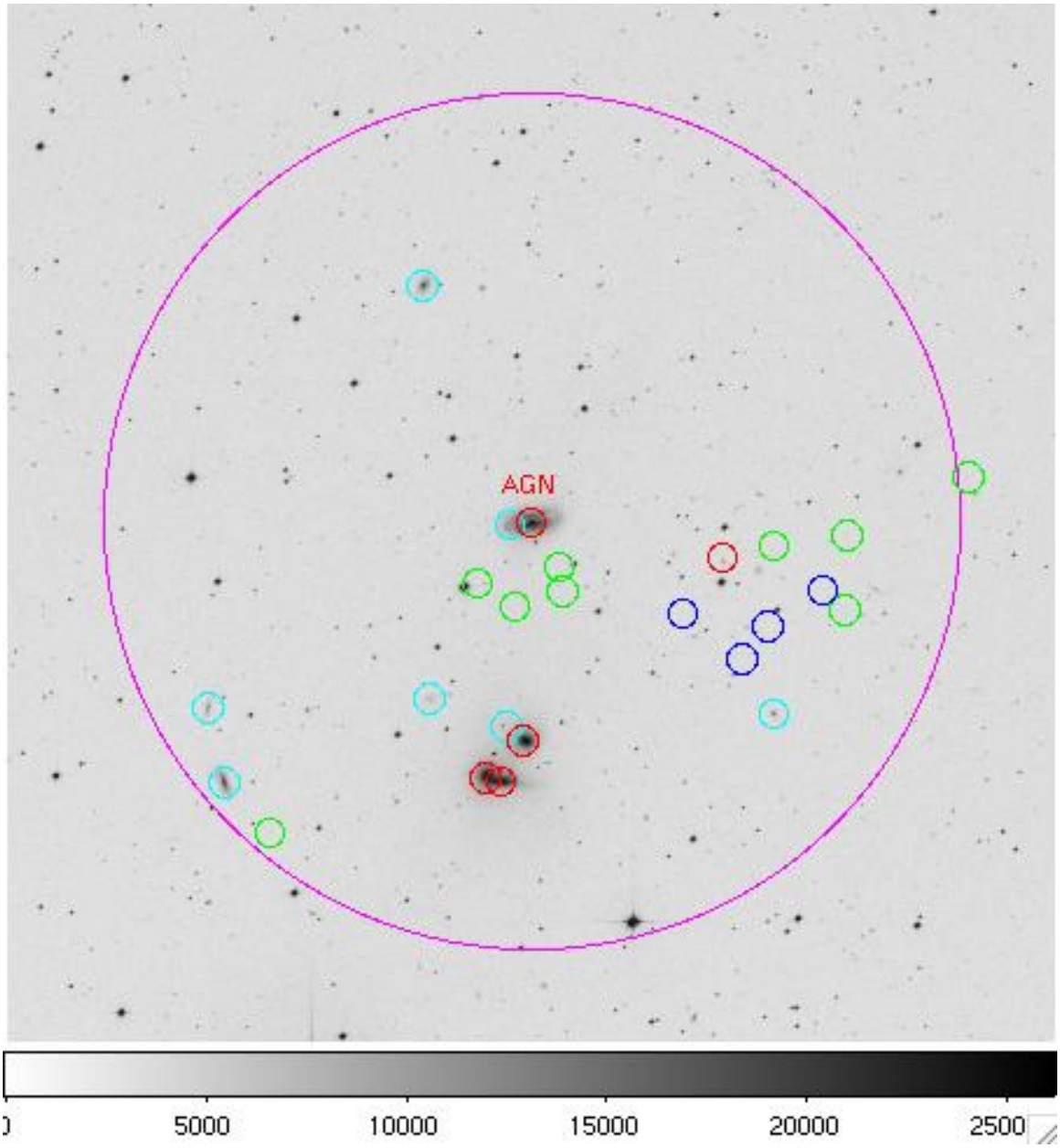

Figure 4.3: The distribution of X-ray sources and the optical galaxies in HCG 90. The circle shown here has a radius of 125 kpc.

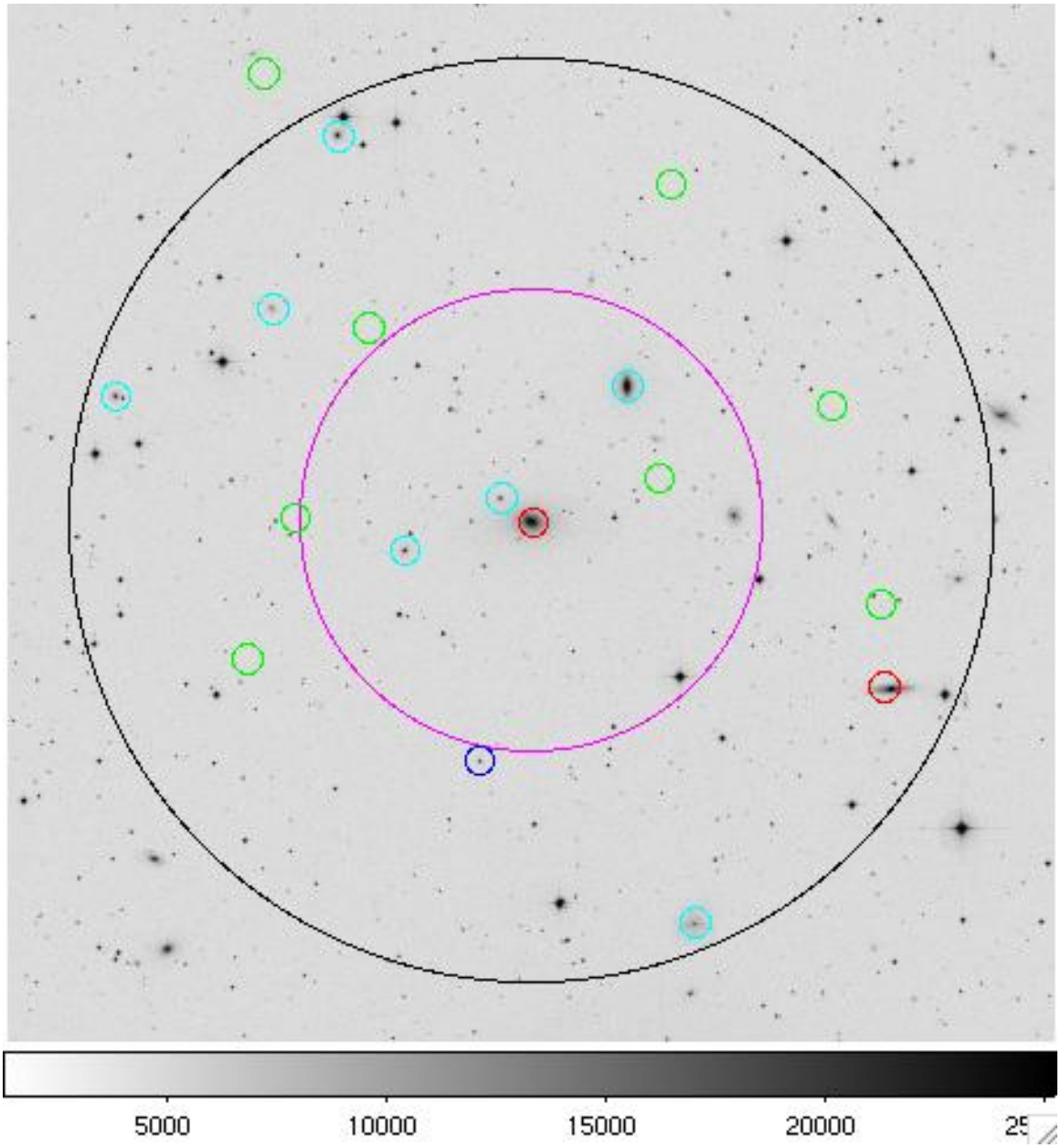

Figure 4.3: The distribution of X-ray sources and the optical galaxies in NGC 2563.

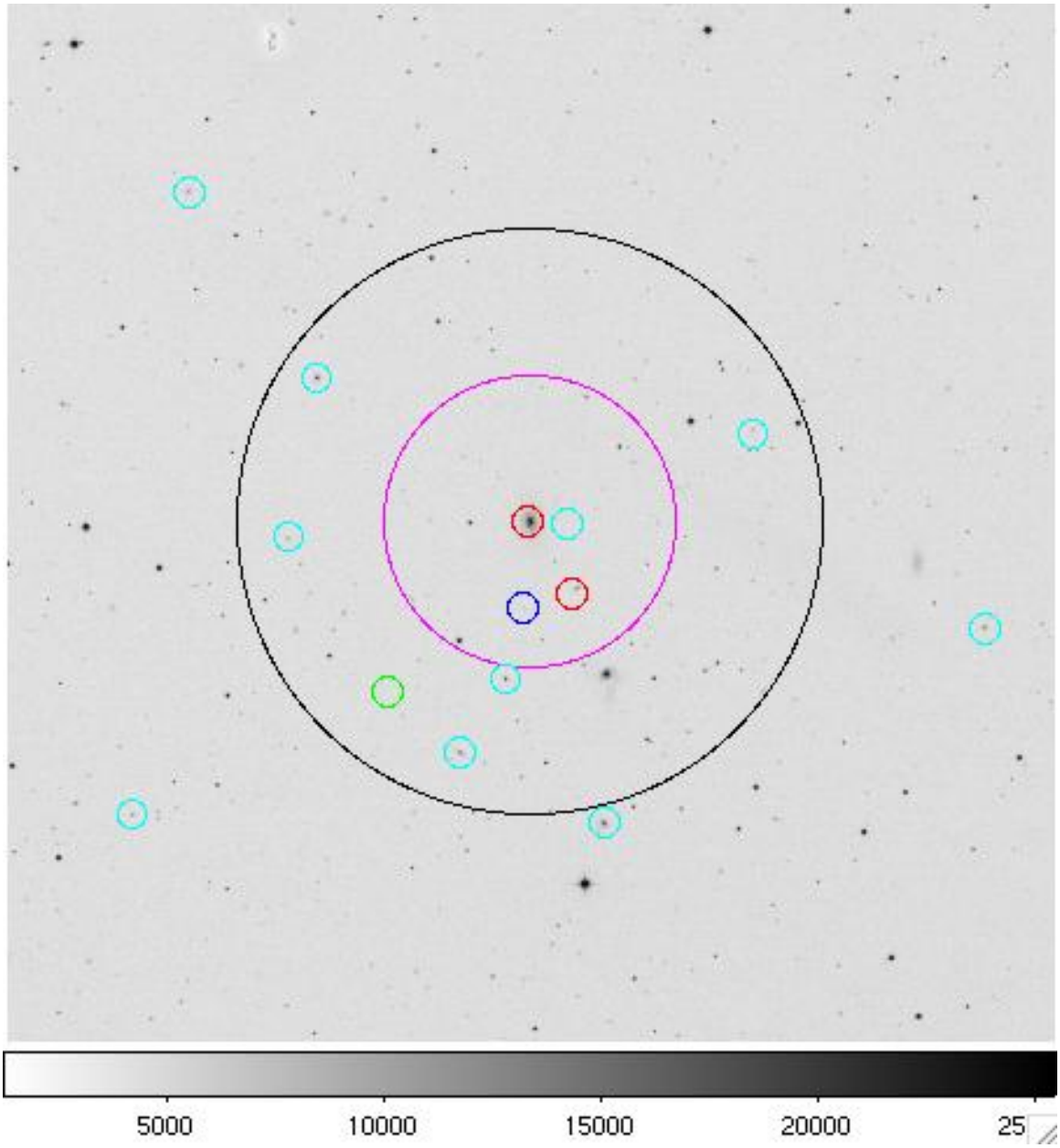

Figure 4.3: The distribution of X-ray sources and the optical galaxies in NGC 4325.

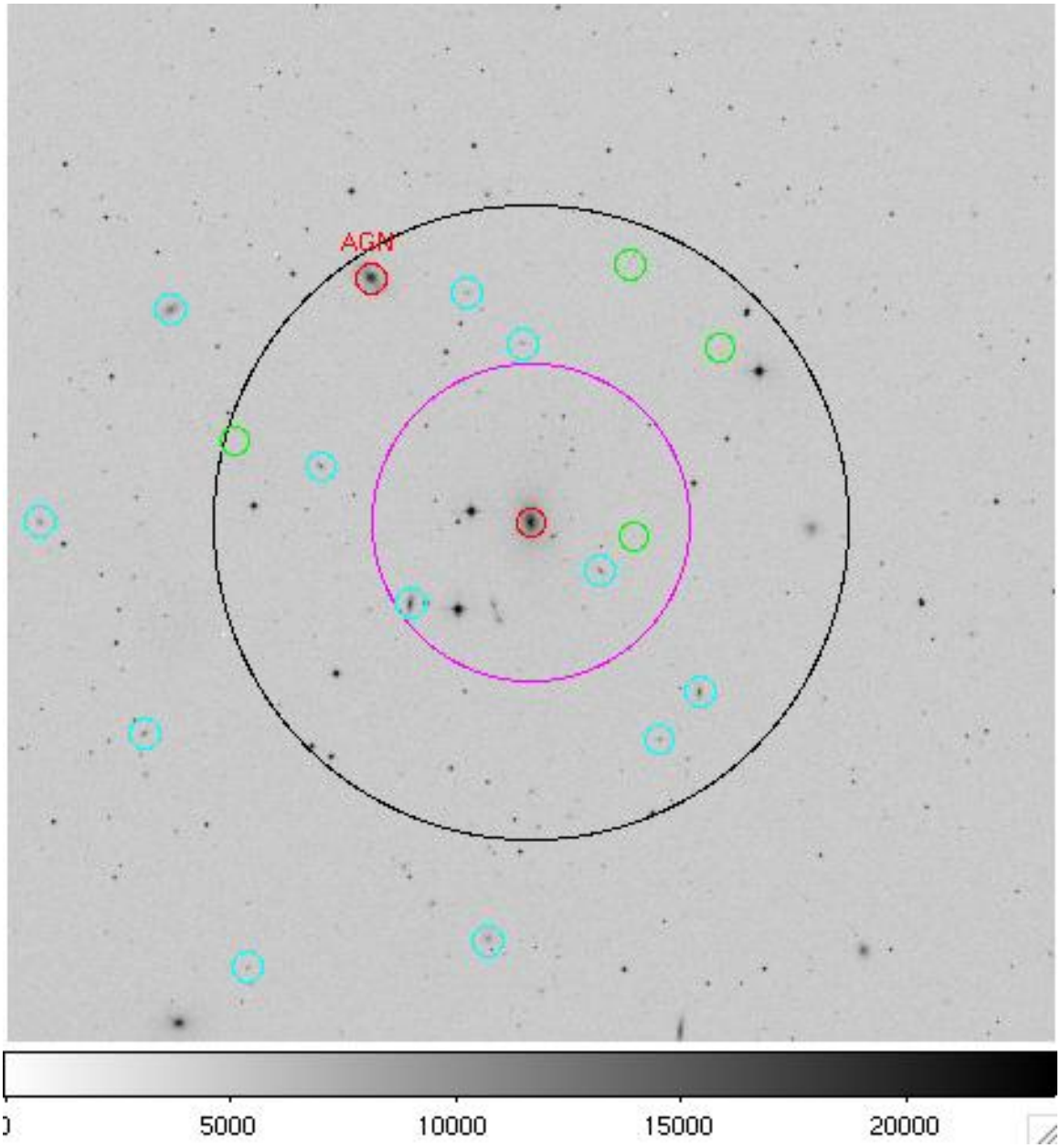

Figure 4.3: The distribution of X-ray sources and the optical galaxies in NGC 5129.

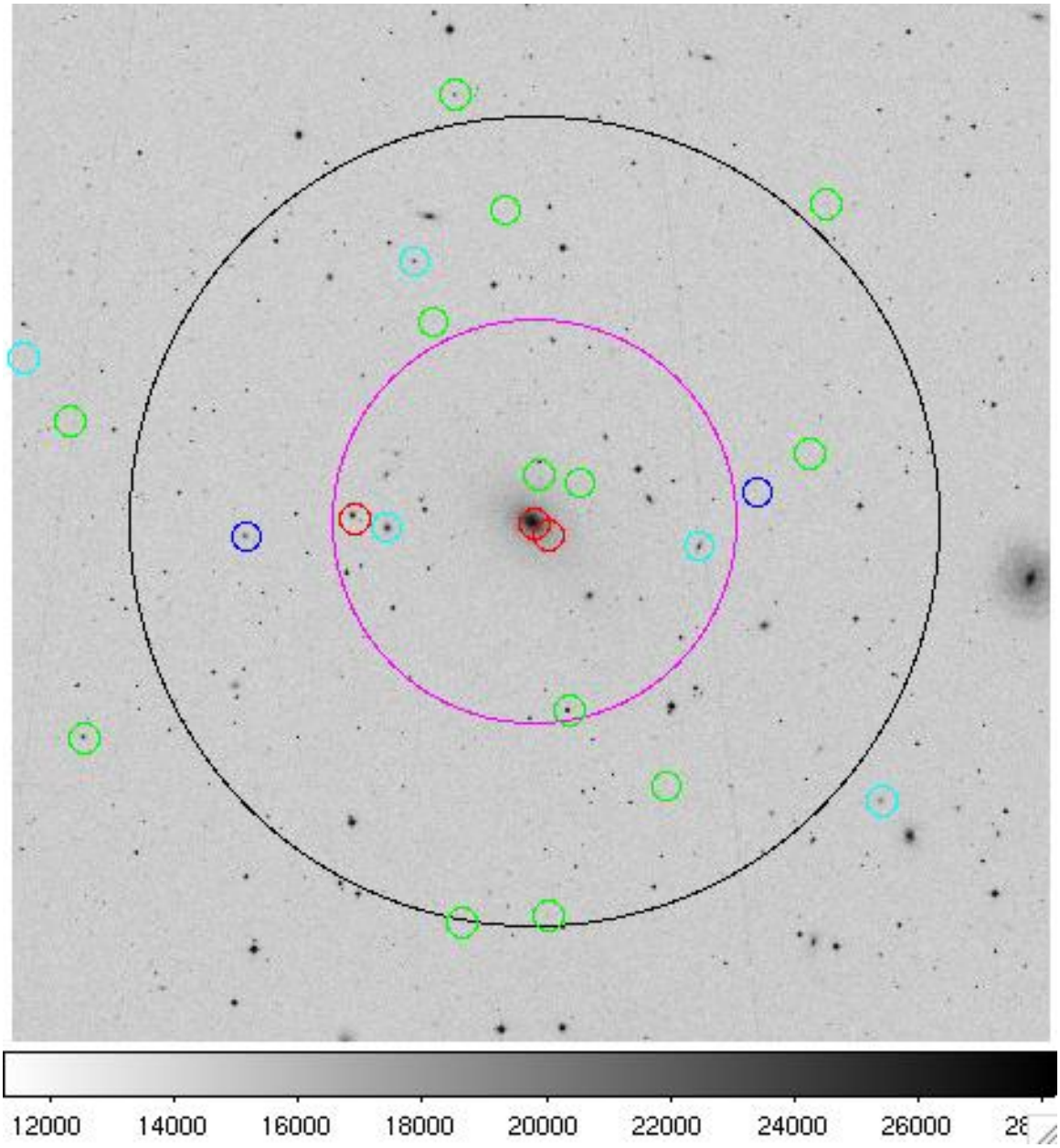

Figure 4.3: The distribution of X-ray sources and the optical galaxies in NGC 533.

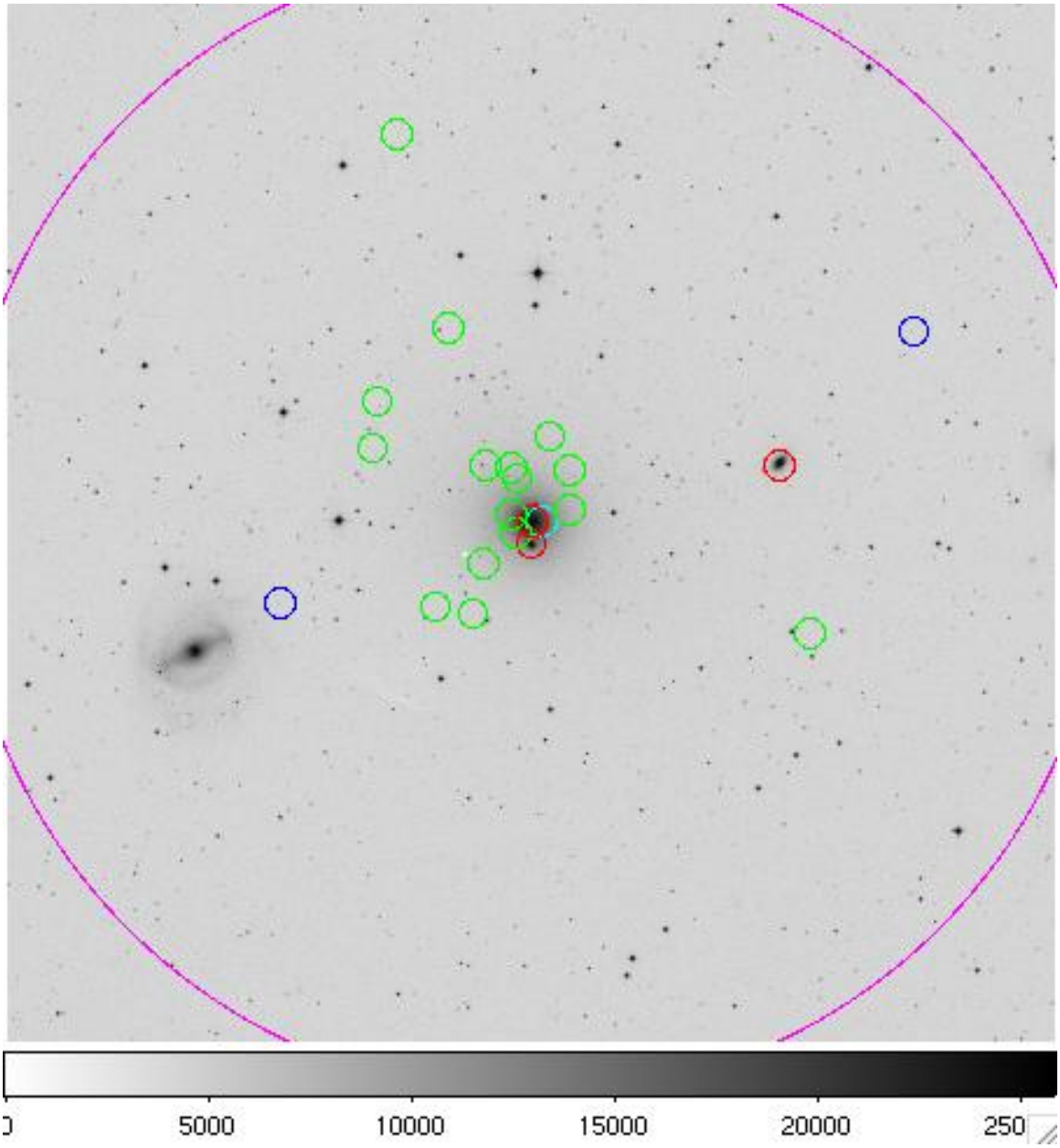

Figure 4.3: The distribution of X-ray sources and the optical galaxies in NGC 5846. The circle here has a radius of 125 kpc.

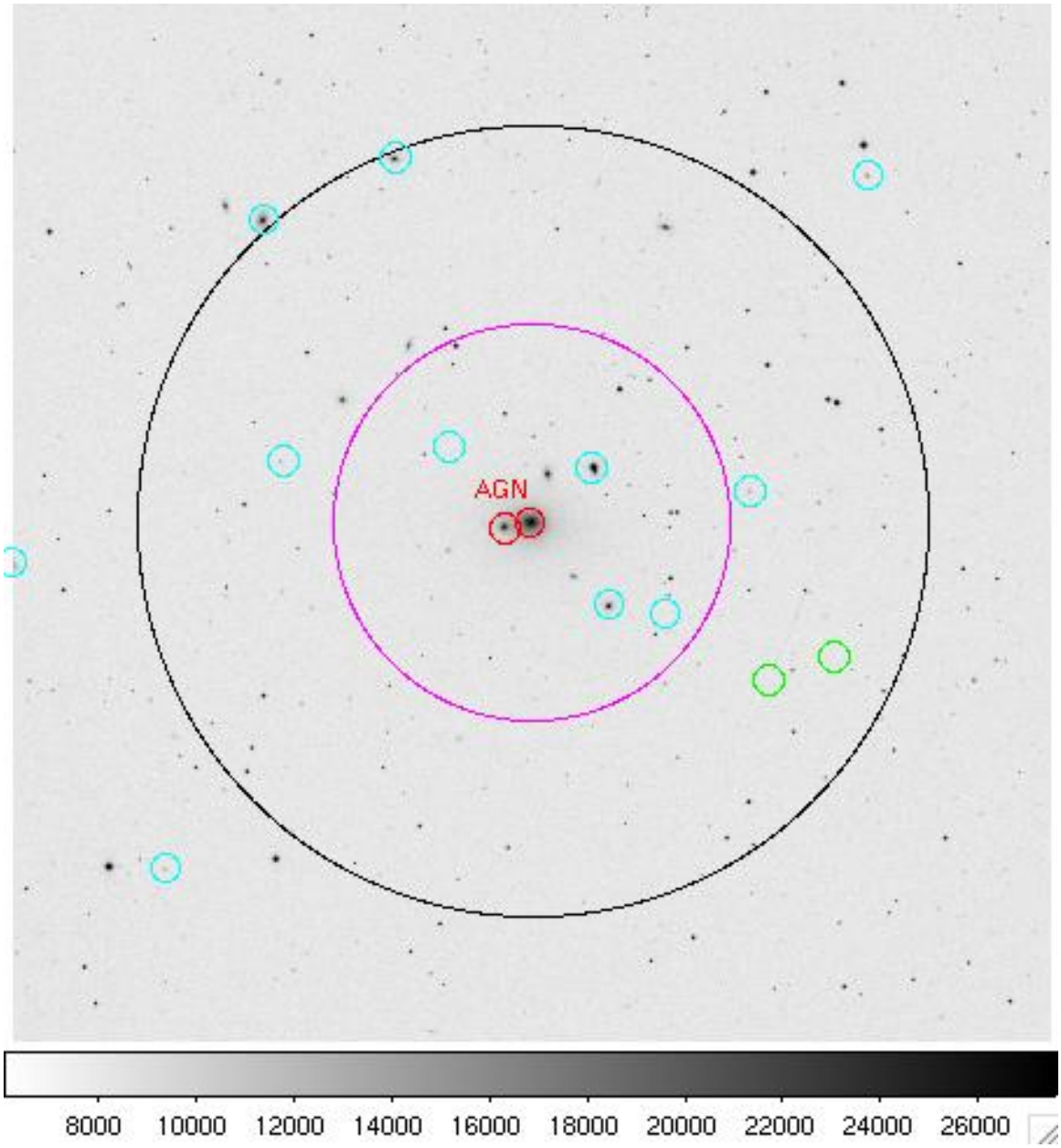

Figure 4.3: The distribution of X-ray sources and the optical galaxies in NGC 741.

CHAPTER 5

Conclusions

We used publicly available data from XMM-Newton to determine the AGN fraction of galaxy groups. Using a sample size of nine groups, we found that three of our X-ray point sources were active galactic nuclei. From this we calculated an AGN fraction $f_A = 11.1^{+13.6}_{-7.0}\%$, with a limiting X-ray luminosity of 10^{41} erg/s and limiting optical magnitude of $M_R = -20$. There was a fourth point source that had an X-ray luminosity higher than the cutoff, but it was not considered to be an AGN based on work by Russell et al. (2007).

Our AGN fraction is slightly higher than that of galaxy clusters found by Martini, which was $\sim 5\%$. It is also slightly higher than Shen's value for groups ($\sim 7\%$). Shen also found that only one of those AGN were identifiable in the X-ray, although all three of ours were detected by XMM-Newton. This is most likely because our groups were all X-ray bright, while only one of his was.

Although the group environment is where galaxies undergo much of their evolution, they are not well studied. We hope the work presented here will help us understand this environment. We also hope to further our knowledge about AGN development in the group environment.

Acknowledgments

This research has made use of the NASA/IPAC Extragalactic Database (NED) which is operated by the Jet Propulsion Laboratory, California Institute of Technology, under contract with the National Aeronautics and Space Administration.

We acknowledge the use of NASA's *SkyView* facility (`http://skyview.gsfc.nasa.gov`) located at NASA Goddard Space Flight Center.

This publication makes use of data products from the Two Micron All Sky Survey, which is a joint project of the University of Massachusetts and the Infrared Processing and Analysis Center/California Institute of Technology, funded by the National Aeronautics and Space Administration and the National Science Foundation.

I would like to thank the Observatories of the Carnegie Institution of Washington and especially Dr. John Mulchaey for taking me on as a summer research student during 2006. Dr. Mulchaey guided me through this project, and working with him at Carnegie reinforced my decision to continue in astronomy. I would also like to thank Dr. Bryan Penprase for introducing me to such a wonderful place.

Additionally, I must thank my advisors, Dr. Alma Zook and Dr. Philip Choi. Dr. Zook has been extremely helpful throughout the years. She has guided me through classes, and kept me on track when I was ready to quit and become an economics major and go to law school. Professor Choi has spent many hours this year helping me craft this thesis and advising me about graduate school. He has

made sure that I did not get too discouraged or too stressed during either of these processes.

Thanks also to Max Wainwright, for looking at this with a fresh pair of eyes.

Lastly, I must thank my parents. They have read this and helped me to proofread it. They have also gotten me through when I was ready to throw my laptop out the window and become a street performer on the Third Street Promenade.

Bibliography

P. Martini, D. D. Kelson, E. Kim, J. S. Mulchaey, and A. A. Athey, ApJ **644**, 116 (2006), `astro-ph/0602496`.

A. Dressler, I. B. Thompson, and S. A. Shectman, ApJ **288**, 481 (1985).

H. Karttunen, P. Kroeger, H. Oja, M. Poutanen, and K. J. Donner, *Fundamental astronomy* (Fundamental astronomy, by Hannu Karttunen, P. Kroeger, H. Oja, M. Poutanen, and K.J. Donner, 4th ed., Berlin: Springer, 2003., 2003).

W. Tucker and R. Giacconi, *The X-ray universe* (Cambridge, MA, Harvard University Press, 1985, 211 p., 1985).

B. W. Carroll and D. A. Ostlie, *An introduction to modern astrophysics* (2nd edition. San Francisco, CA, Pearson, Addison-Wesley, 2007).

W. R. Leo, Nuclear Instruments and Methods in Physics Research B **34**, 290 (1988).

M. Dahlem, *XMM Users' Handbook European Space Agency—XMM Science Operations Centre* (1999).

L. Strüder, U. Briel, K. Dennerl, R. Hartmann, E. Kendziorra, N. Meidinger, E. Pfeffermann, C. Reppin, B. Aschenbach, W. Bornemann, et al., A&A **365**, L18 (2001).

J. Barnes, in *Encyclopedia of Astronomy and Astrophysics*, edited by P. Murdin (Institute of Physics Publishing, Bristol, U.K., 2001), p. 1059.

J. S. Mulchaey, Annu. Rev. Astron. Astrophys. **38**, 289 (2000), `astro-ph/0009379`.

J. Barnes, MNRAS **215**, 517 (1985).

A. I. Zabludoff and J. S. Mulchaey, ApJ **496**, 39 (1998), astro-ph/9708132.

K.-V. H. Tran, L. Simard, A. I. Zabludoff, and J. S. Mulchaey, ApJ **549**, 172 (2001), astro-ph/0010278.

I. Shlosman, M. C. Begelman, and J. Frank, Nature **345**, 679 (1990).

P. Martini, D. D. Kelson, J. S. Mulchaey, and S. C. Trager, ApJ **576**, L109 (2002), astro-ph/0208017.

B. M. Peterson, *An Introduction to Active Galactic Nuclei* (An introduction to active galactic nuclei, Publisher: Cambridge, New York Cambridge University Press, 1997 Physical description xvi, 238 p. ISBN 0521473489, 1997).

J. S. Mulchaey, D. S. Davis, R. F. Mushotzky, and D. Burstein, ApJ **404**, L9 (1993).

S. Snowden, S. Immler, M. Arida, B. Perry, M. Still, and I. Harrus, *The XMM-Newton ABC Guide: An Introduction to XMM-Newton Data Analysis* (2004).

M. F. Skrutskie, R. M. Cutri, R. Stiening, M. D. Weinberg, S. Schneider, J. M. Carpenter, C. Beichman, R. Capps, T. Chester, J. Elias, et al., AJ **131**, 1163 (2006).

P. A. Russell, T. J. Ponman, and A. J. R. Sanderson, ArXiv Astrophysics e-prints (2007), astro-ph/0703010.

N. Gehrels, ApJ **303**, 336 (1986).

Y. Shen, J. S. Mulchaey, S. Raychaudhury, J. Rasmussen, and T. J. Ponman, ApJ **654**, L115 (2007), astro-ph/0611635.